Available online at www.sciencedirect.com
ScienceDirect
Focus Article, *Mendeleev Commun.*, 2013, **23**, 299–312
Mendeleev Communications

Spin hyperpolarization in NMR to address enzymatic processes *in vivo*

Igor V. Koptyug[a,b]

[a] *International Tomography Center, Siberian Branch of the Russian Academy of Sciences, 630090 Novosibirsk, Russian Federation. E-mail: koptyug@tomo.nsc.ru*
[b] *Novosibirsk State University, 630090 Novosibirsk, Russian Federation*

DOI: 10.1016/j.mencom.2013.11.001

Magnetic resonance imaging and spectroscopy are powerful techniques but have a relatively low sensitivity. Signal enhancement in NMR and MRI by several orders of magnitude can be provided by the so-called hyperpolarization methods. Recent achievements in the development of the dissolution dynamic nuclear polarization technique and its use in the studies of enzymatic processes *in vivo* and *in vitro* and other applications are presented. Parahydrogen-induced polarization is also briefly discussed. Finally, recent progress in extending the lifetime of nuclear spin hyperpolarization beyond the relaxation limit is mentioned.

1. Introduction

Modern NMR has a very broad range of scientific and practical applications. One of its most advanced fields is biomedical and/or *in vivo* NMR imaging (MRI) and spectroscopy (MRS). MRI is a powerful tool widely used in current medical diagnostics, while MRS is increasingly used to monitor injected reporter molecules or to detect small metabolites in organs and tissues *in vivo*. Despite its limited spatial resolution, magnetic resonance is rapidly entering the new era of molecular and cellular imaging defined as the visualization and quantification of processes at the cellular and sub-cellular levels in an intact organism.

While an impressive progress has been achieved in numerous applications including *in vivo* MRI and MRS, significant further advance is possible provided that efficient approaches are found to boost the sensitivity of NMR. To address the sensitivity limitations, several techniques grouped under the name 'hyperpolarization' are being actively developed in NMR. One of the promising areas of application of such techniques is biomedical research.[1–3] Among currently available techniques, only dynamic nuclear polarization (DNP) and parahydrogen-induced polarization (PHIP or PASADENA) have already been applied to the *in vivo* studies of enzymatic processes. The use of hyperpolarization techniques improves signal-to-noise ratio (SNR) in MRS and MRI studies by several orders of magnitude. In addition, it provides a researcher with new possibilities. For instance, conventional ^{1}H MRS studies *in vivo* provide information on the steady-state concentrations of detected metabolites. At the same time, in the studies of metabolism the information on the fluxes through various metabolic pathways may be much more relevant than the metabolite concentrations themselves. 'Fluxomics' is a rapidly growing area of research in metabolomics. A combination of conventional MRI and MRS with the hyperpolarization techniques provides kinetic information necessary to evaluate fluxes through various enzymes. Thus, hyperpolarized NMR provides opportunities for the dynamic evaluation of metabolism in normal tissues and organs, for an early detection of various pathologies including cancer, and for the evaluation of a response of a disease to various treatments at early stages when morphological changes are not yet detectable.

2. DNP basics and dissolution DNP

The phenomenon of DNP is known for many years.[4–7] It relies on the fact that unpaired electrons have a much larger magnetic moment than magnetic nuclei; thus, the polarization of electron spins is larger than that of nuclear spins in the same magnetic field and at the same temperature. The necessary ingredients for DNP are a diamagnetic substance to be hyperpolarized and a paramagnetic stable free radical or biradical (or a paramagnetic metal ion). The sample is then placed in a high static magnetic field to polarize electron spins. A microwave magnetic field applied to the electron spins results in the transfer of their polarization to the nuclear spin manifold in the system of interacting spins.

DNP in solution, often referred to as Overhauser effect, can in principle provide ^{1}H NMR signal enhancements of ~660,[7,8] but in practice the efficiency of polarization transfer is limited and the observed enhancements are usually much smaller.[9–14] Solid-state DNP can be performed at much lower temperatures than liquid-phase experiments and thus can provide much higher nuclear spin polarizations. Recent impressive developments in solid-state DNP-enhanced NMR are based on a significant progress achieved over the past 20 years in developing instrumentation and methodology for high-field DNP.[14–16] The new era in the use of DNP for NMR signal enhancement in a liquid phase started fairly recently with the introduction of the so-called 'dissolution DNP'. The ingeniously simple idea of the novel approach was to use solid-state DNP for producing hyperpolarization in a liquid phase.[17,18] In this technique, the droplets of a liquid sample containing a substrate and a radical (usually nitroxyl or trityl) are first rapidly frozen in liquid nitrogen. The sample is then

Igor V. Koptyug received his PhD degree in 1991; in 1992–1995 he was a postdoctoral researcher in the photochemistry group of Professor N. J. Turro (Columbia University, New York). He earned his Dr. Sci. degree in catalysis in 2003 and a title of Professor in 2006; currently, he is the head of the Laboratory of Magnetic Resonance Microimaging at the International Tomography Center, Siberian Branch of the Russian Academy of Sciences, Novosibirsk. His research interests include signal enhancement in NMR and applications of NMR and MRI in catalysis and biological studies *in vivo* and *in vitro*.

transferred to the DNP polarizer where it is maintained at a low temperature (1.1–1.4 K) in a fairly high and uniform magnetic field. Under these conditions, the electron spins are almost fully polarized (~98% at 3.35 T and 1 K). The application of microwaves (*e.g.*, ~94 GHz at 3.35 T) to the frozen sample for 30–120 min gradually transfers the polarization of electron spins to the nuclear spins of the entire solid sample. After that, the solid is rapidly dissolved by injecting a pressurized solvent preheated to boiling temperature, and the sample is transferred to an NMR instrument for measurements. In many reported studies, a commercial DNP instrument (HyperSense, Oxford Instruments) was used, but other designs have been reported[19] including systems intended for medical use.[20,21]

A sample polarized using dissolution DNP yields an SNR enhancement of 10^2–10^4 and more when compared to a thermally polarized sample at room temperature in the same magnetic field. For instance, in the original demonstration of the dissolution DNP technique,[17] polarizations of 37% for ^{13}C and 7.8% for ^{15}N, respectively, were obtained for ^{13}C-labeled urea after dissolution. These polarizations correspond to dramatic signal enhancements of 44 400 for ^{13}C and 23 500 for ^{15}N, respectively, compared with thermal equilibrium at 9.4 T and room temperature. As a result, in many cases, the high-quality NMR spectra of hyperpolarized substances can be obtained using just a single scan; for comparison, the spectra of thermally polarized samples with comparable SNR would have to be accumulated for unreasonable periods of time estimated at ~100 days[22] to ~3200 years.[18] Obviously, the development and optimization of the process is well worth the effort.

In order for the process to work properly, many technical issues have to be addressed and resolved.[23–26] In particular, the sample should form an amorphous glass upon freezing either by itself or upon addition of an appropriate glass-forming solvent (*e.g.*, glycerol). Upon dissolution, the hyperpolarized substance is typically diluted by a factor of 20–100. Therefore, high initial concentrations (~1 mol dm^{-3}) of a substrate are usually required. At the same time, dissolution dilutes the stable radical as well, reducing the paramagnetic line broadening and the rate of hyperpolarization decay. In certain cases including *in vivo* studies, it may be imperative to completely remove the radical after the dissolution stage. Filtration through a short anion-exchange column and reverse phase filtration have been suggested for this purpose.[18] Another demonstrated approach is to add frozen beads of a concentrated solution of ascorbate on top of the frozen sample.[27] After dissolution, the ascorbate is mixed with the hyperpolarized sample and scavenges nitroxide radicals. The use of two immiscible (aqueous and organic) solvents for dissolution has been suggested,[28] so that the minority solvent preferentially dissolves the hyperpolarized substrate at an optimal dilution, and the majority solvent mainly dissolves the radical and is removed from the sample before its use.

The specific feature of the nuclear spin hyperpolarization is its transient nature. In conventional NMR experiments, spin-lattice relaxation of nuclear spins restores the initial equilibrium magnetization after each excitation-detection cycle. In contrast, once the hyperpolarized state is created, it starts to decay irreversibly due to the spin-lattice relaxation. Therefore, the nuclei of hyperpolarized substances should have T_1 times sufficiently long for the hyperpolarization to survive through the dissolution process, injection into a sample tube or an organism, chemical transformation (if reactions are addressed), and the NMR signal detection. Therefore, heteronuclei (^{13}C, ^{15}N, *etc.*) are often preferred to ^{1}H, especially in the studies of chemical transformations, since the T_1 times of protons (seconds) are usually too short for such applications. The most addressed nucleus is ^{13}C. For carbonyl and quaternary carbon atoms, the T_1 times can be fairly long. In the molecules used for *in vivo* studies, the ^{13}C T_1 times are usually in a range from 10 to 40 s *in vivo*. As the initial polarization is often very large, this usually provides a window of ~2–3 min for dissolution, sample transfer to the NMR instrument, detection, and, if present, the reaction. ^{13}C DNP is frequently used in combination with ^{13}C-enriched samples to further increase SNR. At the same time, other ^{13}C atoms present at the natural abundance of 1.1% are often observable in the spectra of hyperpolarized substances. The absence of a background signal from non-polarized molecules may be an additional advantage. Another reason for using heteronuclear NMR is a broader range of chemical shifts, which makes it easier to distinguish different analytes in a mixture or in an organism.

For the studies performed in a sample tube, the sample transfer time between the dissolution in the polarizer and injection into the sample tube positioned in the NMR probe can be as short as 2 s, which makes it possible to acquire NMR spectra for molecules with much shorter T_1 times (larger than ~0.7 s), which includes various magnetic nuclei in most small organic molecules, and even in larger molecules such as polypeptides and even proteins.[22] In the studies of reactions, the delay between the injection and the start of spectrum acquisition is important. The use of a high-pressure injection system makes it possible to obtain a reaction dead-time as short as 300 ms.[29,30] In *in vivo* studies, the added time required for sample administration usually leads to delays of 15–40 s. While the initial hyperpolarization is usually high (5–35% for ^{13}C, compared to the equilibrium polarization of about 8×10^{-4}% at 9.4 T and 37 °C), such long delays lead to substantial polarization losses before the detection can be started. Other specifics of the *in vivo* work require the use of buffered saline for dissolution and temperatures of ~37 °C and pH 7.0–7.5 upon administration. Before the hyperpolarized substance reaches the target organs and tissues after an intravenous (i.v.) injection, its contact with blood can further reduce its T_1. The initial concentrations after dissolution are usually in the range of 2.5–80 mmol dm^{-3}. After dissolution and i.v. injection, the hyperpolarized molecule is diluted *ca.* 100-fold before it reaches the tissue of interest.

In addition to the irreversible relaxation mentioned above, hyperpolarization is also destroyed irreversibly by the applied rf pulses during an NMR or MRI experiment. Therefore, it should be spent wisely. The modern MRI/MRS toolkit allows one to acquire spatial and spectroscopic information, making it possible to detect localized volume-selective NMR spectra, or spatial images of a certain chemical. Multidimensional experiments with the spectral and 1–3 spatial dimensions allow one to acquire NMR spectra from multiple voxels simultaneously and to process such data sets into the maps reflecting the spatial distribution of the detected chemicals. All these possibilities have been combined with hyperpolarization, providing the opportunity to perform rapid multidimensional dynamic MRSI experiments that cover temporal, spectral, and up to three spatial dimensions.[26,31,32]

Dissolution DNP also has a number of disadvantages. DNP in a solid state is a relatively slow process. For heteronuclei such as ^{13}C, the usual duration of the hyperpolarization stage is 1–2 h. It was suggested recently that DNP hyperpolarization of ^{1}H nuclei followed by the Hartmann–Hahn cross-polarization (CP) to low-γ nuclei such as ^{13}C or ^{15}N can greatly accelerate the polarization buildup while simultaneously providing much higher levels of polarization.[27,33] This way, the solid-state polarization for ^{13}C nuclei in excess of 70% was obtained within 20 min.[34] After rapid dissolution, this would correspond to a 120 000-fold signal enhancement at 300 K and 6.7 T. Dissolution DNP is a batch process, which cannot provide a hyperpolarized substance continuously, and is an expensive one. Despite that, the popularity of DNP as a hyperpolarization technique is growing explosively.

3. DNP studies *in vivo* and *ex vivo*

3.1. General considerations. The DNP-enhanced *in vivo* NMR imaging and spectroscopy experiments reported to date can be divided into two categories. The first group deals with the hyperpolarized substances that are metabolized slowly and tend to remain in the blood. These are used to study tissue perfusion and to rapidly obtain high-resolution angiographic images of blood vessels after an i.v. injection of a hyperpolarized solution, as well as for passive catheter tracking in interventional MR.[35–38] Another exciting and challenging possibility is to use hyperpolarized substrates that can be metabolized within the lifetime of nuclear spin hyperpolarization, which is then inherited by the newly formed metabolic products.[23–26,35,36,39–42] When a polarized ^{13}C-labeled substance is injected intravenously, its conversion into other metabolites can be detected, and their spatial distribution can be imaged. This way, the real-time monitoring of important dynamic metabolic processes *in vivo* and the quantification of their kinetics can be performed noninvasively. This can be done not only for normal conditions, but also for a variety of pathologies. Application of this technique beyond normal cell metabolism, and in particular to develop reliable biomarkers for disease progression and evaluation of an early response to treatment, is one of the driving forces of current research. The ability of NMR to address metabolic fluxes rather than changes in metabolic concentrations makes hyperpolarized substances the promising biomarkers for detecting malignant transformations, including tumor progressions and their response to therapy. Numerous technical and practical limitations make the choice of suitable substances for such studies rather non-trivial. About 40 metabolites have been demonstrated to match the relevant criteria, with 10–40% polarization levels achieved.[25]

3.2. Pyruvate metabolism. Most of the published *in vivo* studies address metabolic pathways of [1-^{13}C$_1$]pyruvate using ^{13}C MRS/MRI. In fact, so far it is the only hyperpolarized compound that made it to phase I clinical trials on patients with prostate cancer.[43] Pyruvic acid readily forms an amorphous solid at 1 K; it can be efficiently polarized, and its C1 carbon has a relatively long T_1 in solution (~40 s at 14 T). Pyruvate easily passes into the cytosol where biochemical reactions can take place (Figure 1). In mammalian cells, pyruvate is produced by the glycolytic pathway, and it plays a key role in cellular metabolism. In normal tissue, pyruvate delivered to mitochondria is irreversibly converted into acetyl-coenzyme A (acetyl-CoA) by pyruvate dehydrogenase enzyme complex (PDH) under the regulation by pyruvate dehydrogenase kinase (PDK) and pyruvate dehydrogenase phosphatase (PDP). Acetyl-CoA enters the Krebs (or tricarboxylic acid, TCA) cycle. In addition, the CO_2 produced in the same process is partly converted into HCO_3^-, with the equilibrium depending on tissue pH. Pyruvate is also converted into oxaloacetate by pyruvate carboxylase (PC). In the cytosol, pyruvate is reduced to lactate by lactate dehydrogenase (LDH) and transaminated to L-alanine by alanine transaminase (ALT). Pyruvate fluxes through different enzymes change significantly in many diseased states.

After an i.v. injection, ^{13}C-labeled pyruvate is rapidly distributed in the body and is actively transported into the cells of most organs by monocarboxylate transporters (MCTs), where it is metabolized rapidly with the corresponding incorporation of the hyperpolarized ^{13}C label in its metabolites. Dynamic NMR spectra (Figure 2) and MRI distribution maps (Figure 3) of hyperpolarized [1-^{13}C]pyruvate and its major metabolites [1-^{13}C]alanine, [1-^{13}C]lactate, and [^{13}C]bicarbonate in the organs and tissues of laboratory animals *in vivo* have been reported.[32,44–46] In a number of studies, specific organs were addressed (*in vivo*, or perfused *ex vivo*), including *in vivo* cardiac metabolism in rats,[47] rat brain,[48,49] kidneys,[32,50] and liver.[51]

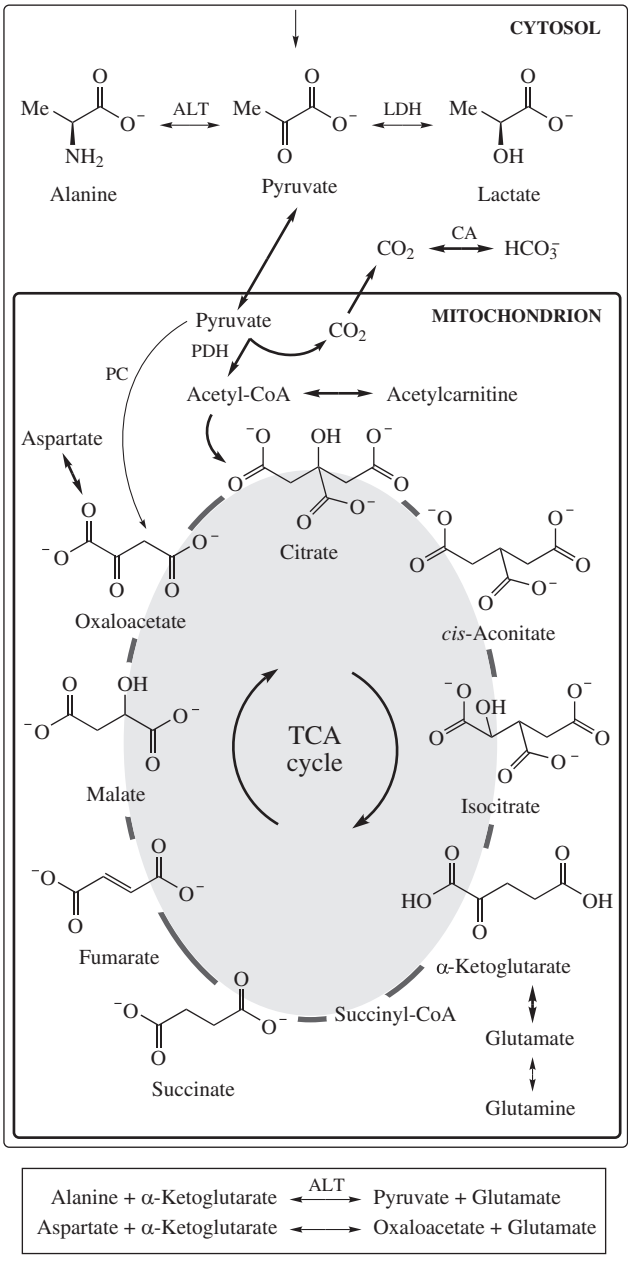

Figure 1 Schematic diagram of metabolic events addressed with NMR of hyperpolarized metabolites. TCA is tricarboxylic acid, ALT is alanine transaminase, LDH is lactate dehydrogenase, CA is carbonic anhydrase, PDH is pyruvate dehydrogenase, PC is pyruvate carboxylase, and CoA is coenzyme A.

It is now recognized that the incorporation of the ^{13}C label in [1-^{13}C]lactate from hyperpolarized [1-^{13}C]pyruvate is not necessarily the result of the net flux through the LDH enzyme. Significant contribution is provided by the reversible nature of the reaction, leading to the exchange of the ^{13}C label between the two metabolite pools. Indeed, after an i.v. injection of hyperpolarized [1-^{13}C]pyruvate, the saturation or inversion of the hyperpolarized [1-^{13}C]lactate NMR signal significantly accelerated the loss of [1-^{13}C]pyruvate signal, demonstrating an efficient flux of the ^{13}C label from lactate to pyruvate.[52] These observations imply that hyperpolarized [1-^{13}C]lactate should be predominantly observed in those tissues which contain significant amounts of lactate, such as tumors, hypoxic tissues or tissues with high rates of glycolysis.

In some cases, the conversion of injected pyruvate into lactate may be determined by the availability of NADH, the reduced form of the coenzyme nicotinamide adenine dinucleotide (NAD+), rather than by the LDH activity. In liver, the levels of NADH

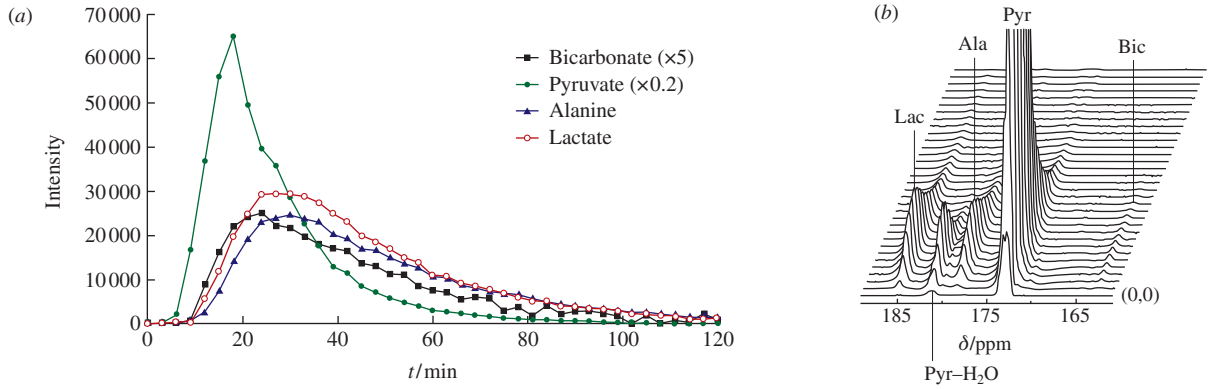

Figure 2 (*a*) Dynamic curves of [1-^{13}C]pyruvate and its metabolic products [1-^{13}C]alanine, [1-^{13}C]lactate, and ^{13}C-bicarbonate following an injection of hyperpolarized [1-^{13}C]pyruvate into a rat. (*b*) A stack of spectra acquired every 3 s from a 90-mm thick section of the rat torso and used to extract the dynamic curves shown in (*a*). Reproduced with permission from ref. 26. © 2012, Wiley Periodicals, Inc.

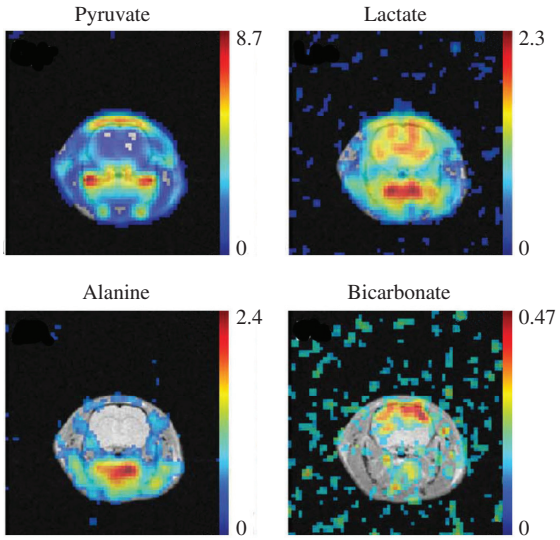

Figure 3 Metabolic maps of a rat head acquired 27 s after the start of injection of [1-^{13}C]pyruvate in the tail vein, superimposed onto the corresponding anatomical image. Data were averaged over four injections. Reproduced with permission from ref. 49. © 2010, Wiley-Liss, Inc.

can be significantly elevated when ethanol is metabolized to acetaldehyde and the latter is converted into acetate. These two reactions are catalyzed by alcohol dehydrogenase (ADH) and acetaldehyde dehydrogenase (ALDH), respectively, and both lead to the transformation of NAD+ to NADH. Accumulation of excess NADH is associated with fatty liver disease, hepatitis, cirrhosis, and hepatocellular carcinoma. Assuming that NADH levels are rate-limiting for liver pyruvate-to-lactate conversion, the activities of ADH and ALDH can be indirectly probed by monitoring the fast conversion of hyperpolarized [1-^{13}C]pyruvate to lactate.[53] A twofold increase in the rate of pyruvate to lactate conversion in the liver was observed in the presence of ethanol, with minimal changes detected in kidney alanine and lactate and liver alanine levels.

Quantitative fluxes through the involved enzymes are obtained using appropriate models to simulate the kinetic data.[54–56] In addition to the substrate delivery to the tissue/organ, transport into the cell and the activity of enzymes, the variation of NMR signals of the substrate and its metabolites in time is also governed by nuclear spin relaxation. Contributions to the NMR signal from the intra- and extracellular pools of metabolites can be distinguished experimentally.[40,57] Pyruvate and other substrates for metabolic *in vivo* MR are usually injected in large doses (*e.g.*, 0.05–1 mmol kg^{-1}) and high concentrations (20–100 mmol dm^{-3}), which exceed physiological concentrations by one to three orders of magnitude[25,35] and may lead to enzyme saturation effects.[50]

Hyperpolarized [1-^{13}C]pyruvate was used in various models of cancer. An example is the transgenic adenocarcinoma of the mouse prostate (TRAMP).[31,58,59] The elevated pyruvate and lactate signals in the vicinity of prostatic tissues and larger lactate-to-pyruvate ratios compared to normal mice were observed. Total hyperpolarized carbon (THC) and alanine were suggested as non-invasive biomarkers of prostate cancer and its histologic grade.[60] In the studies of implanted rat sarcoma, the tumor area was shown to contain the highest concentration of lactate[61] (Figure 4). The metabolism of pyruvate into alanine was dominating in the muscle, but it was very low in the tumor. Significantly greater levels of [1-^{13}C]lactate and [1-^{13}C]alanine in rat hepatocellular carcinoma (HCC) compared with normal liver were observed.[62] The maps of these two metabolites were colocalized with the tumor, demonstrating that the conversion of administered [1-^{13}C]pyruvate to [1-^{13}C]lactate and [1-^{13}C]alanine is a characteristic marker of HCC *in vivo*. *In vivo* localized T_2 measurements revealed that upon injection of hyperpolarized [1-^{13}C]pyruvate in rats with HCC tumors, the T_2 times of produced [1-^{13}C]alanine and [1-^{13}C]-lactate were significantly longer compared to normal liver.[63] The same study reports that the alanine/THC ratio in HCC tumors was significantly higher, while the lactate/THC ratio was similar to that in normal liver.

The early response of tumors to treatment may be accompanied by the reduction in lactate labeling, as observed in various models of cancer[64,65] including rats with implanted human glio-

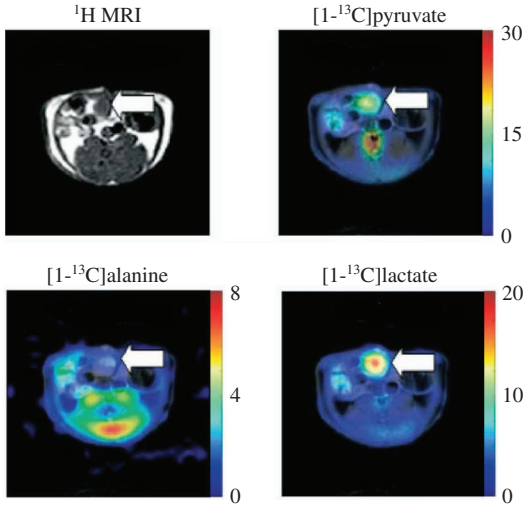

Figure 4 Anatomical ^{1}H MR image of a rat with implanted sarcoma (top left), and the spatial distribution of metabolites after injection of [1-^{13}C]-pyruvate in the tail vein. In all images, the position of the implanted tumor is indicated by a white arrow. All ^{13}C MR images have been individually scaled. Reproduced with permission from ref. 36. © 2006, Elsevier.

blastoma.[66,67] Reduction in the LDH flux in mouse lymphoma cells *in vitro* and in lymphoma tumors *in vivo* was demonstrated after the cell death induced with etoposide.[68] The rate constants obtained by kinetic modeling reflect LDH activity, membrane transport of lactate and pyruvate and, in the *in vivo* studies, pyruvate delivery to the tumor. Images of the tumor before and after treatment reveal heterogeneity in the lactate/pyruvate ratio and a marked reduction of this ratio in the treated tumor. Furthermore, the dominating conversion of pyruvate into alanine in precancerous tissues was detected prior to any observable morphological or histological changes,[69] which is extremely important for the early diagnosis of cancer.

While the production of alanine and lactate reflects the general metabolic activity of the cell, the production of HCO_3^- reflects mitochondrial activity. Decarboxylation of [1-$^{13}C_1$]pyruvate by pyruvate dehydrogenase (PDH) in mitochondria produces $^{13}CO_2$ which is partly converted into $H^{13}CO_3^-$ depending on tissue pH.

Pyruvate is extensively used to address cardiac metabolism[70,71] because its metabolic conversion can be significantly altered by ischemic conditions or mitochondrial dysfunction, diabetes, hypertension, ischemia and reperfusion, *etc*. Metabolic imaging with hyperpolarized [1-^{13}C]pyruvate simultaneously provides information on regional perfusion (pyruvate distribution map), cellular damage (alanine map) and mitochondrial energy production (bicarbonate map). Modulation of PDH activity in the cardiac muscle cells of lab animals was observed under different ischemic conditions,[72] in starved and diabetic rats,[73] upon *in vivo* administration of drugs,[74,75] *etc*.

The labeled carbon atom of [1-^{13}C]pyruvate is eliminated as $^{13}CO_2$ when pyruvate is converted into acetyl-CoA. In contrast, the use of [2-^{13}C]pyruvate is expected to result in the formation of [1-^{13}C]acetyl-CoA, which enters the TCA cycle upon its conversion to form [2-^{13}C]citrate and thus provides access to TCA cycle intermediates. The use of hyperpolarized [2-^{13}C]pyruvate in isolated perfused rat hearts resulted in the observation of its metabolic products including [5-^{13}C]glutamate, [1-^{13}C]citrate, [1-^{13}C]acetylcarnitine, [2-^{13}C]lactate and [2-^{13}C]alanine.[76] The changes in metabolite concentrations following ischemia and reperfusion were monitored. The study of [2-^{13}C]pyruvate metabolism in real time simultaneously provided information on glycolysis ([2-^{13}C]lactate), PDH flux and energy demand ([1-^{13}C]acetylcarnitine) and a defined part of the TCA cycle ([1-^{13}C]citrate ↔ ↔ isocitrate → α-ketoglutarate → [5-^{13}C]glutamate). All of the observed enzymatic conversions occurred within 5 s of [2-^{13}C]-pyruvate arrival at the coronary arteries, and [5-^{13}C]glutamate was detected 3 s later than [1-^{13}C]citrate appearance. Spontaneously hypertensive rats (SHR) were studied as a model of hypertension and hypertrophy to monitor the adaptation of cardiac metabolism using both [1-^{13}C]- and [2-^{13}C]pyruvic acid.[77] The former demonstrated the increased PDH flux into CO_2 and bicarbonate pools in the SHR heart compared with control. Incorporation of the ^{13}C label from [2-^{13}C]pyruvate was increased by 72% into citrate, 118% into acetylcarnitine, and 81% into glutamate in the SHR heart. The possibility to use [1,2-$^{13}C_2$]pyruvate to simultaneously observe the downstream metabolites of both PDH flux and TCA cycle flux with a single dose of the hyperpolarized substrate was demonstrated in the pig heart *in vivo*.[78]

The HCO_3^-/CO_2 ratio observed upon administration of [1-^{13}C]-pyruvate was used for *in vivo* assessment of intracellular pH (pH_i) in the myocardium in the study on isolated rat hearts before and immediately after ischemia.[79] In healthy living rats *in vivo*, pH_i was evaluated as 7.20±0.03 from the $H^{13}CO_3^-/^{13}CO_2$ ratio. The same approach was used to estimate pH_i in the SHR heart.[77]

In liver, PDH flux may be insignificant. Nevertheless, pyruvate can enter the TCA cycle efficiently *via* its carboxylation to oxaloacetate by pyruvate carboxylase (PC). This was confirmed in isolated perfused murine liver[80] by the observation of hyperpolarized [1-^{13}C]malate, [1-^{13}C]aspartate and smaller amounts of [4-^{13}C]malate and [4-^{13}C]aspartate within seconds after administration of hyperpolarized [1-^{13}C]pyruvate, and indicated a partial equilibration with fumarate within the TCA cycle. The observed ^{13}C enrichment in the 4-positions of malate and aspartate indicates the involvement of the reversible conversion of malate into fumarate, which randomizes the ^{13}C label between the 1- and 4-positions. Therefore, their ratio contains information on the kinetics of the malate–fumarate equilibrium as part of the TCA cycle dynamics. These results demonstrate the ability of hyperpolarization to survive through up to six enzymatic reactions.

The use of hyperpolarized substances is also promising for assessing neurodegenerative diseased states. It was observed that a measurable amount of [1-^{13}C]pyruvate passes normal blood-brain barrier (BBB) during the first passage of an injected bolus, and the formation of ^{13}C-bicarbonate and [1-^{13}C]lactate in the brain tissue was observed[26,49] (Figure 3). Kinetic modeling was used to determine the fluxes through LDH and PDH in the brain and the rate of transport of pyruvate through the BBB.[48] Injection of hyperpolarized [2-^{13}C]pyruvate resulted in the observation of only [2-^{13}C]lactate in an intact rat brain. Lipophilic ethyl pyruvate (EP) is expected to cross the BBB significantly faster. Indeed, in the studies using [1-^{13}C]-EP in a normal rat brain *in vivo*,[81] it was observed that, in contrast to pyruvate, EP is characterized by a rapid and preferential uptake into the brain. Its conversion to lactate and bicarbonate and hydrolysis to pyruvate were successfully detected.

3.3. Metabolism of other substrates. Further insight into the metabolic processes may be provided using hyperpolarized substrates other than pyruvate. Hyperpolarized [1-^{13}C]alanine was used to study the flux through ALT *in vivo* in the heart and liver of a healthy mouse.[82] Lactate, pyruvate and bicarbonate were detected within 60 s of injection, with lactate giving the strongest signal. Upon injection of hyperpolarized [1-^{13}C]alanine, it was found that in normal rat tissue the lactate/pyruvate ratio was more than 10 times higher as compared to [1-^{13}C]pyruvate injection.[83] This points to the fact that when pyruvate is used, the majority of detected pyruvate is extracellular, whereas the transformation of hyperpolarized alanine to pyruvate and then lactate requires alanine transport into the cell; thus, the levels of pyruvate and lactate reflect intracellular values only, and they are independent of perfusion and uptake through MCTs. In addition, nine other [1-^{13}C]amino acids (Asp, Cys, Gln, Glu, Gly, Leu, Lys, Met and Ser) were hyperpolarized as prospective biomarkers for the *in vivo* assays of transaminase activity,[82] but the T_1 times were found to be very short at basic pH in a low magnetic field.

Glutamate is an important metabolite involved in nitrogen transport and is the major excitatory neurotransmitter. Alterations in glutamate metabolism are associated with neurodegenerative disease, stroke, brain injury, *etc*. The reaction catalyzed by ALT transfers an amino group from glutamate to pyruvate yielding alanine and α-ketoglutarate (αKG). The latter is an intermediate in the TCA cycle, and it plays an important role in cancer. Thus, monitoring the dynamics of glutamate and αKG could be useful in biomedical applications. L-[1-^{13}C]glutamic acid was hyperpolarized and used to demonstrate the formation of αKG both *in vitro* and *in vivo*.[84] Formation of αKG from [1-^{13}C]glutamate observed in human hepatoma cells supported on microcarrier beads was shown to increase significantly by incubating the cells with pyruvate. In the experiments performed *in vivo* using murine lymphoma implanted in mice, the formation of αKG could be detected only when hyperpolarized glutamate was coinjected with sodium pyruvate. Both experiments demonstrate that the intracellular pyruvate concentration is limiting for the reaction catalyzed by ALT.

The reverse enzymatic conversion of hyperpolarized [1-^{13}C]-lactate into the pyruvate pool and subsequent metabolism of the latter were addressed using hyperpolarized [1-^{13}C]lactate in rats.[85] The metabolisms of pyruvate and lactate were compared in rat heart upon the administration of dichloroacetate.[86] As the endogenous pyruvate pool is much smaller than that of lactate, the label exchange after an injection of ^{13}C-labeled lactate is less efficient compared to the injection of ^{13}C-labeled pyruvate.

The pH value in normal tissue is maintained rigorously but is altered by many pathologies such as cancer, ischemia and inflammation. Therefore, the detection of diseased states and response to treatment can be based on the observation of changes in tissue pH. As the $H^{13}CO_3^- \leftrightarrow {}^{13}CO_2$ equilibrium is pH-dependent, the ratio of their signal intensities following an i.v. injection of hyperpolarized $H^{13}CO_3^-$ can be used to measure the tissue pH. The exchange reaction is catalyzed by carbonic anhydrase enzyme (CA), but it can be relatively fast even in its absence. At the same time, on the NMR timescale the exchange is slow, and the two ^{13}C NMR signals are observed separately and can be readily quantified. This approach was used in a mouse tumor (subcutaneous lymphoma) model, and the average tumor pH was found to be significantly lower than that in the surrounding tissue[87] (Figure 5). Exchange between $H^{13}CO_3^-$ and $^{13}CO_2$ was confirmed by selectively saturating the $^{13}CO_2$ resonance, which led to the loss of polarization of $H^{13}CO_3^-$. When carbonic anhydrase was inhibited with acetazolamide, such selective saturation did not result in any decrease in the $H^{13}CO_3^-$ signal. A comparison with the results obtained with an extracellular ^{31}P MRS pH probe, 3-aminopropylphosphonate, indicated that bicarbonate is predominantly sensitive to the extracellular pH (pH_e). Indeed, both approaches reflected changes in tumor pH induced by modulating systemic pH. Hyperpolarized bicarbonate predominantly reports on the pH_e value in tumors because its concentration after the injection is significantly higher in the extracellular volume, and possibly because the nuclear spin relaxation times may be shorter in the intracellular space.[88]

In contrast to pH measurements based on the bicarbonate injections, the use of pyruvate considered earlier provides access to the intracellular value of pH (pH_i).[88] Production of carbon dioxide from pyruvate takes place in mitochondria; therefore,

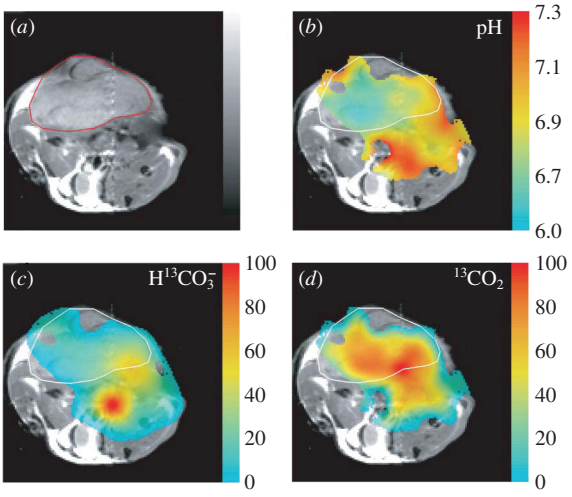

Figure 5 (*a*) Transverse proton magnetic resonance image of a mouse with a subcutaneously implanted lymphoma (outlined). (*b*) pH map of the same animal calculated from the ratio of the voxel intensities in ^{13}C chemical shift images of (*c*) $H^{13}CO_3^-$ and (*d*) $^{13}CO_2$ acquired ~10 s after an i.v. injection of ~100 mmol dm^{-3} hyperpolarized $H^{13}CO_3^-$ and assuming a pK_a of 6.17. The spatial distribution of (*c*) $H^{13}CO_3^-$ and (*d*) $^{13}CO_2$ are in percent of the respective maximum values. The tumor margin in (*b*), (*c*) and (*d*) is outlined. Reproduced with permission from ref. 87. © 2008, Macmillan Publishers, Ltd.: NATURE.

CO_2 and its conversion into bicarbonate are initially intracellular. The diffusion of CO_2 out of mitochondria into the cytosol will result in a pH_i being a weighted average of the cytosolic and mitochondrial pH. For this approach to work, high activities of both PDH (*e.g.*, in the heart) and CA are required.

Attempts to probe the activity of multiple enzymes simultaneously have been reported. The simultaneous polarization and subsequent administration of [^{13}C]bicarbonate and [1-^{13}C]-pyruvate was used to perform both pH and metabolic mapping *in vivo* using a single i.v. bolus injection.[89] Increased levels of lactate and more acidic pH (6.6–7.0) were found in the prostate tumor as compared to benign tissues in TRAMP. The technique was subsequently extended to polarize four ^{13}C-labeled substrates, namely, [1-^{13}C]pyruvic acid, sodium [^{13}C]bicarbonate, [1,4-$^{13}C_2$]-fumaric acid, and [^{13}C]urea, to show the potential of obtaining information on pH, metabolism, necrosis and perfusion in a single *in vivo* imaging experiment.[89]

Hyperpolarized [1,4-$^{13}C_2$]fumarate can be used to detect pathological states that involve cell death (*e.g.*, tumor treatment, toxic insults and ischemia). Fumarate is hydrated by fumarase to malate in TCA. In normal cells, hyperpolarized malate is not observed because of the slow transport of fumarate through a plasma membrane. In necrotic cells, however, the transport should be much faster; thus, the rapid conversion of fumarate to malate may provide a positive marker of tumor cell necrosis even at its early stage. After injection of hyperpolarized [1,4-$^{13}C_2$]-fumarate into tumor cell suspensions and tumor-bearing mice,[90] the production of hyperpolarized [1,4-$^{13}C_2$]malate was monitored in real time. In isolated lymphoma cells treated with etoposide, a 19-fold increase in the conversion rate of fumarate to malate was observed. At the same time, the rate of malate production was unaffected by coadministration of succinate, which competes with fumarate for transport into the cells. Measurements performed *in vivo* in tumors about 24 h after drug treatment showed a 2.4-fold increase in the rate of malate production with the hyperpolarized malate predominantly localized within the tumors. Similar results were obtained in a preliminary study with a human breast tumor cell line. Therefore, the formation of hyperpolarized ^{13}C-labeled malate from [1,4-$^{13}C_2$]fumarate can be potentially used to detect the early response of tumors to treatment.[90] It was demonstrated[91] that both hyperpolarized [1-^{13}C]pyruvate and [1,4-$^{13}C_2$]fumarate are sensitive markers of tumor response to treatment with combretastatin-A4-phosphate (CA4P), the water-soluble prodrug that induces a rapid shape change in proliferating endothelial cells by disrupting microtubule assembly, leading eventually to apoptotic endothelial cell death and disruption of tumor vasculature followed by the necrosis of tumor cells. The increased rate of hydration of [1,4-$^{13}C_2$]fumarate to [1,4-$^{13}C_2$]-malate was evident as early as 6 h after the drug administration.[91] The use of [1,4-$^{13}C_2$]fumarate in human breast adenocarcinoma cells has shown that at 24 h after treatment of the cell culture with doxorubicin, the hyperpolarized ^{13}C malate/fumarate ratio increased by a factor of 5.4 indicating the onset of tumor cell necrosis.[92] In the *in vivo* experiments with the cells introduced subcutaneously in immunodeficient mice, the production of hyperpolarized [1,4-$^{13}C_2$]malate from [1,4-$^{13}C_2$]fumarate initiated by cell necrosis was observed after 72 h post-treatment. In addition, a treatment-induced decrease in labeled lactate production upon injection of [1-^{13}C]pyruvate was observed, which correlated with the decrease in the concentration of the cellular NAD(H) coenzyme pool. The experiments revealed the treatment response in the absence of any changes in tumor size.

Hyperpolarized [2-^{13}C]fructose was used in TRAMP to demonstrate difference in the uptake and metabolism in tumor regions relative to surrounding tissue.[93] Good SNR spectra of hyperpolarized fructose and its metabolite β-fructofuranose-

6-phosphate were obtained, with the latter colocalized in high lactate regions within the tumor. The composite β-fructofuranose and β-fructofuranose-6-phosphate resonance was higher in the malignant lobe of prostate as compared to the benign side.

Acetate is readily taken up by the brain and is metabolized only in astrocytes. Therefore, it can be used to study glial metabolism *in vivo*. Hyperpolarized sodium [1-^{13}C]acetate or sodium [1,2-$^{13}C_2$]acetate were studied in a rat brain *in vivo*.[94,95] Conversion of acetate to α-ketoglutarate (αKG) in the TCA cycle resulted in the NMR signals of [5-^{13}C] αKG or [4,5-$^{13}C_2$] αKG, respectively.[94] This demonstrates that the polarization of the ^{13}C label can survive through several successive enzymatic transformations and acetate could be a sensitive biomarker for neurological disorders.

The redox status of tumors is a key factor in tumor development, response to treatment and drug resistance. In addition, oxidative stress is associated with many other diseases. At the same time, the controlled chemistry of reactive oxygen species (ROS) plays an important role in normal tissues. Ascorbic acid (AA) is an essential antioxidant and a cofactor of numerous enzymes. Most cells uptake the oxidized form of vitamin C, dehydroascorbic acid (DHA), through the action of glucose transporters, which are overexpressed in most tumors. The subsequent intracellular reduction of DHA proceeds through glutathione- (GSH) and NADPH-dependent reactions, both depending on NADPH and altered in tumor cells. As the interconversion of the reduced and oxidized forms of vitamin C *in vivo* is rapid, hyperpolarized [1-^{13}C]AA and [1-^{13}C]DHA were studied as the potential probes of tumor redox states.[96] Extracellular oxidation of [1-^{13}C]AA and intracellular reduction of [1-^{13}C] DHA were observed in the suspensions of hypoxic murine lymphoma cells. The reduction of [1-^{13}C]DHA was also detected in lymphoma tumors *in vivo*, while no oxidation of [1-^{13}C]AA was detected. This is consistent with the notion that the upregulation of antioxidant systems in tumors leads to the reduced microenvironment. Similar *in vivo* studies in rats and mice revealed the rapid conversion of [1-^{13}C]DHA to AA in kidneys, liver, and also in TRAMP tumor compared to normal prostate,[97] confirming the expectation that the reduction should be fastest in tissues with high GSH concentrations and in glycolytic tissues. DHA is also known to cross BBB readily. Indeed, the injection of hyperpolarized [1-^{13}C]DHA into a normal rat led to its significant reduction to [1-^{13}C]AA in the brain, with essentially no conversion observed in the surrounding tissue (Figure 6).

4. DNP studies of cell cultures and purified enzymes *in vitro*

Undoubtedly, the studies *in vitro* provide more flexibility in manipulating the conditions and allow one to separate kinetic and transport effects. At the same time, surprisingly, the number of such studies is much smaller than that of *in vivo* works. Most of them deal with hyperpolarized [1-^{13}C]pyruvate.

Metabolism of [1-^{13}C]pyruvate in immortalized rat hepatoma cells encapsulated in 500 μm alginate beads was addressed to measure LDH and ALT fluxes in real time.[98] To this end, one milliliter of the hyperpolarized pyruvate solution was injected in the medium recirculating in a bioreactor with supported cells, resulting in a final concentration of 2–14 mmol dm^{-3} of pyruvate. The production of lactate and alanine was observed to scale with cell concentration, as expected. The authors concluded that perturbations induced in metabolic fluxes as small as 5% can be measured in the bioreactor. In the studies of human breast cancer cells supported on polystyrene beads,[99] it was concluded that the rate of pyruvate metabolism to lactate reflected the rate of transport from the extracellular medium into the cytoplasm rather than the activity of LDH enzyme. Indeed, the addition of an MCT inhibitor revealed the dose-dependent inhibition of the pyruvate-to-lactate conversion. It was also shown that a vigorous perfusion of the bioreactor 20–30 s after the injection of [1-^{13}C]-pyruvate resulted in its very rapid washout from the medium, whereas, while the polarization lasted (~1 min), the synthesized lactate remained in the cells. The perfusion system used is also well suited for investigating the effects of systematic environmental changes (*e.g.*, oxygen supply, nutrition and added chemicals) on the tumor cells metabolism. For instance, hypoxia induced an increase in the rate of lactate synthesis as early as 4 h after its initiation and persisted throughout the entire experiment. Incubation of hyperpolarized [3,3,3-D_3, 1,2,3-$^{13}C_3$]pyruvate with porcine heart ALT and glutamate[100] led to the transient accumulation of the hyperpolarized methyl carbon of alanine. In addition, ALT catalyzed H/D exchange in the methyl group of alanine. In a later study, the conversion of hyperpolarized [1-^{13}C]pyruvate into lactate in the suspensions of intact and lysed murine lymphoma cells including cells with altered LDH expression was addressed to determine quantitatively the enzyme activity and the rate of membrane transport.[56] Kinetic modeling revealed that both processes have significant control of the observed flux of the ^{13}C label in this particular case.

Hyperpolarized [1-^{13}C]acetate was added to a solution containing multiple components including acetyl-CoA synthetase, coenzyme A and ATP.[101] In addition to the substrate and the products (*Z*- and *E*-acetohydroxamate), the ^{13}C NMR spectra revealed the presence of acetyl-adenylate and acetyl-CoA. These intermediates rapidly achieved relatively low steady-state levels due to their participation in a fast subsequent reaction with hydroxylamine. The results demonstrate the potential of the technique to quickly and quantitatively detect the signals of various molecular species including short-lived intermediates in consecutive and competing reactions. The approach was further extended to study the multistep enzymatic process in which the acetyl-CoA synthetase reaction was followed by the citrate synthetase reaction, with oxaloacetate used as a cosubstrate to yield citrate. The concentrations of acetate, acetyl-CoA and citrate were evaluated as a function of time. The authors argue that, in such experiments, concentrations above 20 μmol dm^{-3} should be detectable without ^{13}C enrichment.

Owing to the important role of glutamine as a cellular energy source, transporter and source of nitrogen, and in synthesis of amino acids and proteins, it plays a key role in tumor cell metabolism. Hyperpolarized [5-^{13}C]glutamine was used to address its metabolism[102] either with the purified enzyme glutaminase

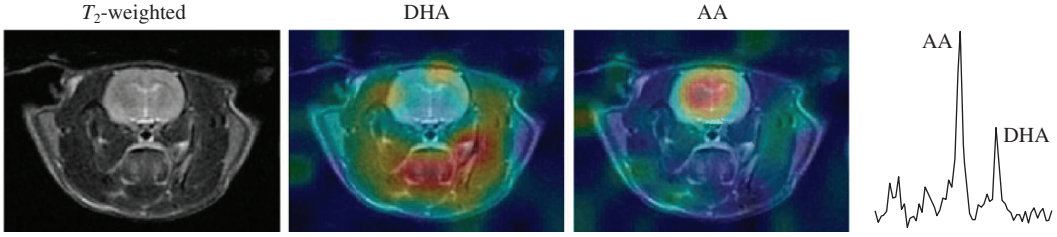

Figure 6 Axial T_2-weighted images and corresponding overlays of hyperpolarized dehydroascorbic acid (DHA) and ascorbic acid (AA) signals in a rat with normal brain. Reproduced with permission from ref. 97. © 2011, National Academy of Sciences of the USA.

from *E. coli* or with intact human hepatoma cells grown on microcarrier beads. Formation of [5-^{13}C]glutamate was observed. Removing the effect of glutamine transport by lysing the cells significantly increased the rate of labeled glutamate production, while the addition of a glutaminase inhibitor markedly reduced it. In addition to the labeled compounds, the signals of the ^{13}C label at natural abundance in [1-^{13}C]glutamate and [1-^{13}C]glutamine were also detectable.

[2-^{13}C]Fructose (T_1 ~ 16 s at 37 °C) was used for *in vivo* hyperpolarized metabolic studies of glycolysis[93] because glucose has very short T_1 times of ^{13}C nuclei (< 1 s). The ^{13}C NMR spectrum of hyperpolarized [2-^{13}C]fructose showed the signals belonging to α-fructofuranose, β-fructofuranose and β-fructopyranose. In the presence of hexokinase and ATP, formation of fructose-6-phosphate was observed.

Phosphorylation of choline by choline kinase is an important step in the production of lipids for cell membranes, which is upregulated in cancerous cells. ^{15}N-labeled hyperpolarized choline was used to demonstrate in real time its metabolic conversion to hyperpolarized ^{15}N-phosphocholine *in vitro* using purified human choline kinase and ^{15}N NMR.[103] The polarization level achieved for the ^{15}N nucleus of choline (~4.6%) provided an enhancement factor of 13 940 at 9.4 T and 25 °C, and the long T_1 time in human blood (120 s at 37 °C).[103] In addition, hyperpolarization of the ^{15}N nucleus can be transferred to protons followed by ^{1}H NMR signal detection.[104] Phosphorylation of choline by choline kinase led to an increase in the phosphocholine peak.[105] The same approach was demonstrated for hyperpolarized ^{15}N-acetylcholine hydrolysis by acetylcholine esterase, a process important for neuronal transmission. Changes in the choline–acetylcholine interconversion have been found in Alzheimer's and Parkinson's diseases. The ^{15}N peaks of acetylcholine and choline are separated by only ~0.05 ppm (2.5 Hz at 11.7 T), and they cannot be reliably resolved by direct ^{15}N detection. Transferring the hyperpolarization to the methylene protons of the 2-CH_2 group of acetylcholine resolves this problem, as the ^{1}H signals of these methylene groups in the two compounds are 0.4 ppm apart.[105]

The bacterial enzyme carboxypeptidase G2 (CPG2) is an example of an exogenous enzyme addressed in the context of targeted chemotherapeutic strategies for converting nontoxic prodrugs into cytotoxic drugs in tumors. 3,5-Difluorobenzoyl-L-glutamic acid (3,5-DFBGlu) undergoes CPG2-mediated conversion into 3,5-difluorobenzoic acid (3,5-DFBA) and L-glutamic acid (L-Glu). 3,5-DFBGlu hyperpolarized to ~ 5% was added to a solution containing CPG2 enzyme.[106] The decay of the hyperpolarized signal from the parent compound was accompanied by the appearance of the ^{13}C NMR signals of 3,5-DFBA and L-Glu.

The kinetics of the hydrolysis of hyperpolarized N_α-benzoyl-L-arginine ethyl ester (BAEE) into N_α-benzoyl-L-arginine by the serine protease enzyme trypsin[29] was studied by detecting a series of single-scan ^{13}C NMR spectra over a period of 3 s. The authors concluded that DNP allows one to use enzyme concentrations about 10 μmol dm^{-3}. The injection system allowed one to start the detection 300 ms after the reaction was initiated by mixing the components. BAEE was not ^{13}C-enriched in these experiments.

The yeast *Saccharomyces cerevisiae* is a widely used eukaryotic model system, and its glycolytic pathway activity has economic importance. The real-time DNP NMR assay was able to follow more than twelve enzyme-catalyzed transformations from uniformly (U) labeled glucose ([U-D, U-^{13}C]glucose) injected in the cell suspension to the catabolic end products ethanol and CO_2.[107] The main glycolytic intermediates observed were fructose-1,6-bisphosphate (Frc-1,6P_2), dihydroxyacetone phosphate (DHAP) and pyruvate, while 6-phosphogluconate (6-PGA) accumulated as the main intermediate of the oxidative pentose phosphate pathway. Injection of [2-^{13}C]fructose revealed the formation of [2-^{13}C]glucose-6-phosphate (Glc-6P) and [5-^{13}C]-Frc-1,6P_2. The NMR detection allows one to resolve molecular subspecies such as carbohydrate α and β anomers as well as free keto acids and their hydrates.

A similar study was carried out with the model prokaryote *Escherichia coli* BL21 (Figure 7).[108] Mixing of the hyperpolarized [U-D, U-^{13}C]glucose with cells suspension resulted in the rapid appearance of the metabolite signals including 6-PGA, Frc-1,6P_2, DHAP, pyruvate, acetyl-CoA, lactate, alanine, acetate, formate, CO_2, bicarbonate, ribulose-5P and ethanol, which attain maxima at different times. Experiments performed with *E. coli* at different growth phases showed that the differences were most pronounced in the signal of 6-phospho-d-gluconolactone (6-PGL) produced in the reaction catalyzed by glucose 6-phosphate dehydrogenase (G6PDH), the first reaction in the oxidative branch of the pentose phosphate pathway. Addition of 2,4-dinitrophenol resulted in the dominating signal of 6-PGL. The signals of ethanol and formate were significantly reduced while pyruvate and CO_2/bicarbonate formation was enhanced.[108] Two different strains of *E. coli* (K-12 and BL21) were compared.[109] In *E. coli* K-12, the signal of 6-PGL was absent because of its ⩾ 30-fold faster hydrolysis as compared to BL21 strain. Furthermore, differences in the glucose metabolism in living *E. coli* and *S. cerevisiae* were addressed as well,[108] in particular, showing more efficient alcoholic fermentation to CO_2 and ethanol in the latter.

Mammalian enzyme aminoacylase-1 hydrolyzes N-acetylated amino acids in kidneys. Deacetylation of hyperpolarized *N*-acetyl-L-[1-^{13}C]methionine to [1-^{13}C]methionine was successfully observed both with the purified aminoacylase-1 enzyme and in the cells (both intact and cell lysate) transfected with the human aminoacylase-1 gene.[110] The study demonstrates the potential to address reporter genes artificially introduced into an organism.

5. DNP studies of non-enzymatic chemical reactions

At present, there are not many examples of such applications. The demonstration of an application of dissolution DNP to an organic reaction is the study of the Diels–Alder reaction of hyperpolarized 1,4-diphenylbutadiene (DPBD) with 4-phenyl-1,2,4-triazole-3,5-dione monitored by ^{1}H NMR.[111] The reaction was observed to carry over the polarization of ^{1}H nucleus to the product. The kinetics of the signals of the product and reactant were modeled to extract the reaction rate constant and the relaxation rate of the product nuclei.

A more advanced example is the detection of reaction intermediates in the living anionic polymerization of styrene in dioxane with sodium naphthalenide as an initiator.[112] Styrene was prepolarized with DNP before the reaction, leading to the signal enhancement of ~4000 in the ^{13}C NMR spectra. The progress of the polymerization reaction was monitored for 13 s through a series of excitations with a small flip angle. Several peaks that were present only during the reaction were assigned to the di-anionic polystyryl intermediate based on the analysis of the resolved multiplet patterns in the ^{13}C NMR spectra. In addition, the assignment was verified using a selective inversion of hyperpolarized peaks of the reactant: the corresponding inverted peaks were observed in the spectrum of the intermediate as this label was passed to the intermediate when the styrene molecule was added to a growing chain. The results convincingly demonstrated that continuous incorporation of hyperpolarized monomers into the growing polymer chain can lead to a selective and renewable hyperpolarization of the active living site of the growing polymer. This provides NMR with a sufficient sensitivity to monitor the living species without signal averaging or stable isotope labeling. By modeling the observed kinetics, the chain propagation rate constant (5.6±0.6 dm^3 mol^{-1} s^{-1}) and the nuclear spin

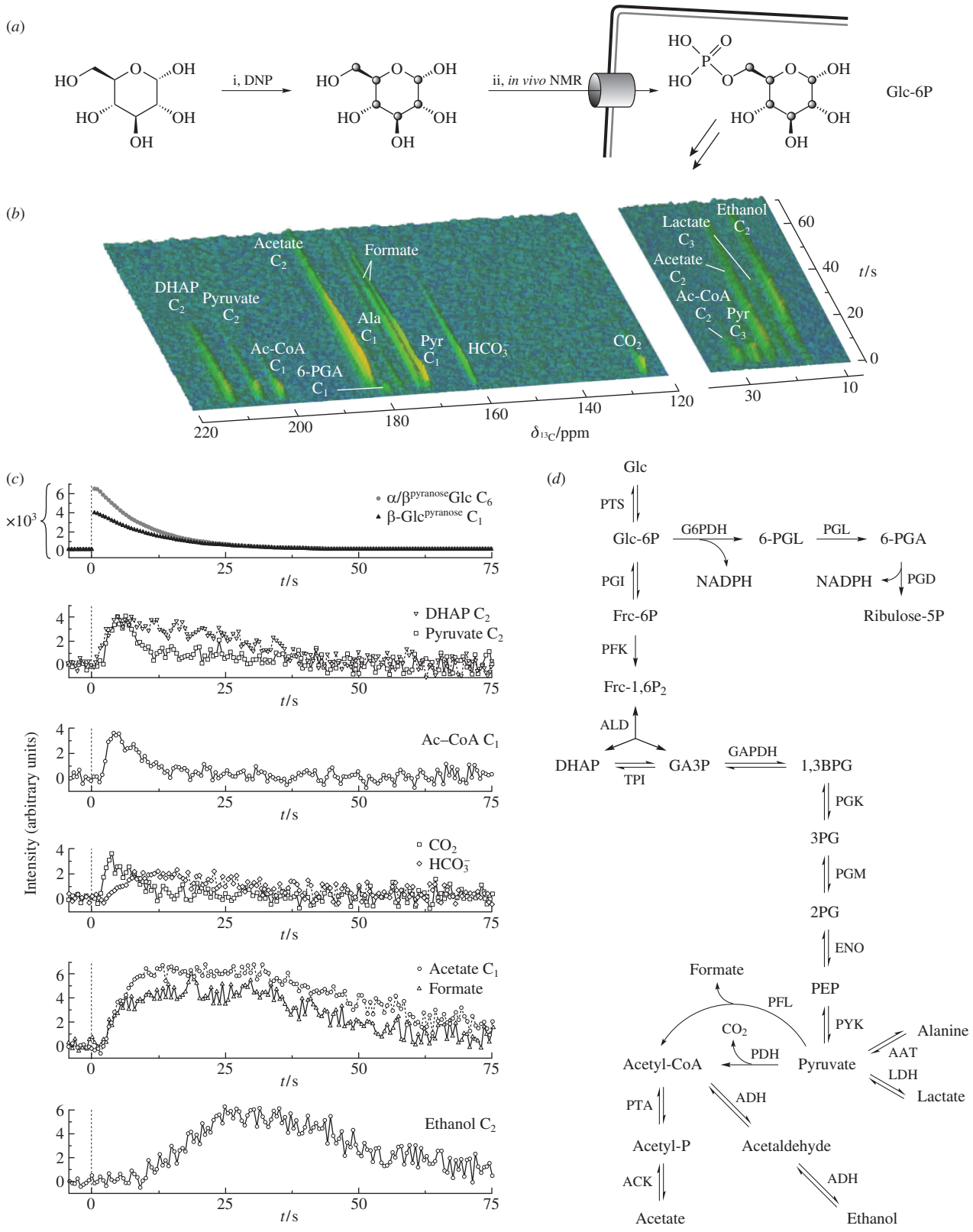

Figure 7 (*a*) Instantaneous pulse-response measurements of microbial metabolism with a pulse of hyperpolarized [U-D, U-^{13}C]glucose fed to a cell suspension of *E. coli* BL21 yielding only signals of the hyperpolarized substrate and its metabolites. (*b*) The set of one-dimensional ^{13}C NMR spectra detected every 0.5 s (150 spectra are shown). Time of substrate injection is defined as $t = 0$ s. (*c*) Temporal evolution of substrate and metabolite signal areas corrected for polarization losses. Signals from major intermediates and products of glycolysis and fermentation are shown. (*d*) Overview of glycolysis, pentose phosphate pathway and mixed acid fermentation reactions in *E. coli* followed in real time. Glc is glucose, PTS is glucose-specific enzyme II of the phosphotransferase system, Glc-6P is glucose-6-phosphate, G6PDH is glucose-6-phosphate dehydrogenase, 6-PGL is 6-phospho-d-gluconolactone, PGL is 6-phosphogluconate lactonase, 6-PGA is 6-phosphogluconate, PGD is 6-phosphogluconate dehydrogenase, Frc-6P is fructose-6-phosphate, PGI is phosphoglucose isomerase, Frc-1,6P$_2$ is fructose-1,6-bisphosphate, PFK is phosphofructokinase, DHAP is dihydroxyacetone phosphate, GA3P is glyceraldehyde 3-phosphate, ALD is aldolase, TPI is triosephosphate isomerase, 1,3BPG is 1,3-bisphosphoglycerate, GAPDH is glyceraldehydes-3-phosphate dehydrogenase, 3PG is 3-phosphoglycerate, PGK is phosphoglycerate kinase, 2PG is 2-phosphoglycerate, PGM is phosphoglycerate mutase, PEP is phosphoenolpyruvate, ENO is enolase, PYK is pyruvate kinase, AAT is alanine aminotransferase, LDH is lactate dehydrogenase, PDH is pyruvate dehydrogenase, PFL is pyruvate formate lyase, ADH is alcohol dehydrogenase, PTA is phosphotransacetylase, ACK is acetyl kinase. Reproduced with permission from ref. 108. © 2011, Elsevier.

relaxation rates were evaluated.[112] Hyperpolarized ethyl-2-cyanoacrylate with tetramethylethylenediamine as an initiator were used to demonstrate a very rapid formation of long hyperpolarized poly(ethyl-2-cyanoacrylate) chains.[22]

Reactive oxygen species (ROS) are important to monitor in many pathological states. In particular, H_2O_2 is a potentially valuable diagnostic marker. 2-Oxo-2-phenyl-[2-^{13}C]acetic acid was hyperpolarized and reacted with H_2O_2 *in vitro*, demonstrating the possibility to detect micromolar levels of this ROS selectively by monitoring its oxidative decarboxylation to benzoic acid.[113] Hyperpolarized *p*-anisidine with a $^{13}CD_3$ group was suggested as a potential ROS biomarker that selectively targets HOCl, the biomarker of inflammation.[114] Its reaction with HOCl led to the formation of $^{13}CD_3OH$.

Dissolution DNP is also a valuable tool for NMR signal enhancement in the absence of chemical reactions. Analytical applications involve the analysis of liquid samples containing low concentrations of analytes that cannot be detected by conventional NMR, in particular, when multidimensional NMR is required.[115–117] Analysis of amino acid mixtures can be performed by reacting them with hyperpolarized acetic anhydride to produce hyperpolarized *N*-acetyl adducts.[118] This secondary hyperpolarization approach was also applied to several small peptides and *N*-acetylcysteine. DNP-based analysis of biological fluids was demonstrated using the quantification of the carbamazepine drug and its metabolic products in blood plasma.[119] Hyperpolarization of polypeptides with ^{13}C NMR signal enhancements of 300–2000 was reported.[120] Ligand–protein interactions have been studied.[121,122] Clearly, many other potential applications can be envisioned. In parallel to the field of dissolution DNP, the interest in the use of DNP in combination with the solid state NMR of frozen hyperpolarized samples is currently growing rapidly,[16,123,124] including studies of biomolecules, biosolids and surfaces of porous and non-porous solid materials.

6. PHIP

Another hyperpolarization technique which is being actively pushed toward the *in vivo* studies of metabolism, is parahydrogen-induced polarization (PHIP, or PASADENA).[125–128] PHIP relies on a catalytic process that involves parahydrogen (pH_2), one of the two nuclear spin isomers of H_2 with the total nuclear spin of two H atoms $I = 0$. A highly correlated state of nuclear spins of pH_2 can be converted into an NMR signal enhancement by removing the equivalence of the two H atoms when pH_2 participates in a suitable chemical reaction. Conventionally, this is done by using a homogeneous hydrogenation reaction of suitable unsaturated precursors catalyzed by transition metal complexes. Once the two H atoms from pH_2 occupy non-equivalent positions in a molecule, the original correlation of their nuclear spins can transform into their polarization. This polarization can be further transferred to other nuclei (^{1}H, ^{13}C, ^{15}N, ^{19}F, *etc*.) coupled to the two hydrogens, either spontaneously or by appropriately manipulating the external magnetic fields.

In contrast to DNP, which utilizes a physical process to polarize nuclear spins, in PHIP, the hyperpolarization is generated in a chemical (catalytic) reaction. Thus, PHIP is a highly sensitive NMR-based tool that can be used to study the mechanisms and kinetics of homogeneous hydrogenations catalyzed by transition metal complexes in solution.[129–131] In addition to the detection of reaction products, the high sensitivity provided by PHIP enables the detection of short-lived reaction intermediates that are normally present at concentrations that are beyond the NMR detection limit. This becomes possible as the symmetry of H_2 in a catalytic cycle is often broken as early as the formation of a dihydride complex and other intermediates accompanied by a dramatic enhancement of their NMR signals.

Immobilization of transition metal complexes on suitable porous solid supports is a viable approach to observe PHIP in the heterogeneous hydrogenation of unsaturated substrates.[132–136] In addition, surprisingly, supported metal nanoparticles were also demonstrated to give pronounced PHIP effects.[137] It was believed earlier that metal surfaces are unable to achieve the required incorporation of both H atoms of an H_2 molecule into the same product molecule because of the dissociative chemisorption of H_2 and rapid surface migration of the resulting H atoms. Despite that, PHIP effects were successfully observed in hydrogenations catalyzed by supported metals,[132,138–141] which significantly expands the scope of potential applicability of PHIP and provides an opportunity to develop a powerful hypersensitive NMR-based technique for the characterization of the heterogeneous catalytic processes of practical importance. A combination of PHIP with MRI makes it possible to study processes in model catalytic reactors and microreactors.[142,143]

In addition to the studies of catalytic hydrogenations, PHIP can be employed in the same way as DNP, namely, as a prepolarization technique to produce highly polarized fluids for their use in spectroscopic and imaging studies including *in vivo* applications. The very first *in vivo* PHIP study was based on the homogeneous hydrogenation of dimethyl acetylenedicarboxylate with parahydrogen catalyzed by a cationic rhodium complex in acetone to produce dimethyl maleate followed by polarization transfer from ^{1}H to ^{13}C nuclei in the reaction product by magnetic field cycling. The resulting cocktail was injected into the tail vein of a rat, and the angiographic ^{13}C MR image of blood vessels was acquired in less than a second.[144] A number of subsequent *in vivo* angiographic studies used different ^{13}C-labeled hyperpolarized substances.

For the *in vivo* studies of metabolism (Figure 1), hyperpolarized [1-^{13}C]succinate was considered. It can be produced by hydrogenating either [2,3-D_2, 1-^{13}C]fumaric acid[145–147] or [1-^{13}C]acetylenedicarboxylate (*via* [1-^{13}C]maleate).[148] After an arterial injection, the hyperpolarized ^{13}C-labeled succinate was observed in the head and cerebral circulation of both normal and tumor-bearing rats but not in the brain or brain tumor.[148] In cancer models in mice, the metabolic conversion of [1-^{13}C]succinate into [1-^{13}C]-malate, [4-^{13}C]malate, [1-^{13}C]fumarate, [1-^{13}C]glutamate and [6-^{13}C]citrate has been detected.[149]

Hyperpolarized diethyl [2,3-D_2, 1-^{13}C]succinate was suggested and used for the real-time *in vivo* MRS studies of the TCA cycle.[150] To this end, diethyl [2,3-D_2, 1-^{13}C]fumarate was hydrogenated with pH_2 to diethyl [2,3-D_2, 1-^{13}C]succinate in an aqueous solution of a Rh catalyst, producing a hyperpolarization level of 2.1% (^{13}C NMR signal enhancement of 5000). After the injection of diethyl [2,3-D_2, 1-^{13}C]succinate into normal mice, malate, succinate, fumarate and aspartate were detected *in vivo*, indicating that a significant fraction of the hyperpolarization of ^{13}C nuclei is retained through three or more enzymatic reactions. Exposure of the animal to an irreversible inhibitor of succinate dehydrogenase (3-nitropropionate) clearly altered the metabolism of diethyl succinate, reducing the signal of succinate. The spatial location of hyperpolarized molecules in the animal after injections was visualized using ^{13}C MRI. The T_1 time of diethyl [2,3-D_2, 1-^{13}C]succinate *in vivo* was about 40 s.

For practical applications including *in vivo* studies, PHIP has a number of advantages over DNP. It is a much cheaper and simpler technique. Furthermore, with PHIP technique the polarized substances can be generated in 3–5 s, as compared to 20–90 min in DNP. Currently, the instrumental implementation of PHIP is based on the homogeneous hydrogenation of unsaturated precursors using transition metal (mostly Rh) complexes as catalysts. For *in vivo* applications, sample preparation in an aqueous medium is required; therefore, the catalysts should

be water-soluble. To achieve a rapid and complete conversion of the precursor into the hyperpolarized substrate, the solution containing the catalyst and the precursor is sprayed into a volume containing pressurized and preheated pH_2. After a few seconds, the liquid is collected, and polarization is transferred from ^1H to ^{13}C nuclei either by cycling the static magnetic field[151–153] or by applying an appropriate sequence of rf pulses.[147,153–155] The entire procedure takes ~5 s, with polarization levels of 15–50% reported for ^{13}C NMR, corresponding to signal enhancements of more than 10^5 at 1.5 T.

For *in vivo* applications, the catalyst should be removed after the hyperpolarization stage. The proven ability of heterogeneous catalysts to produce PHIP effects provides a potential solution to this problem. Indeed, the heterogeneous hydrogenation of unsaturated precursors with pH_2 makes it possible to implement a simple, continuous and rapid production of clean hyperpolarized substances, which represents a significant potential advantage of PHIP over DNP for biomedical applications. In addition, in contrast to homogeneous processes, heterogeneous hydrogenation can be used to produce hyperpolarized gases. However, these advantages are yet to be fully exploited.

A disadvantage of PHIP is that a limited number of stable unsaturated precursors is available, which limits the range of substrates that can be hyperpolarized in a hydrogenation process. Nevertheless, many other molecules have been synthesized and used in PHIP experiments. Examples include sequential hydrogenation of ethyl propiolate to ethyl acrylate and ethyl propionate, and ethyl phenylpropiolate to ethyl cinnamate.[156] Glucose derivatives with a butynoic acid residue moiety provide the triple bond for hydrogenation.[157] Hydrogenation of ^{15}N-propargylcholine with pH_2 followed by the polarization transfer step provided ^{15}N NMR signal enhancement for ^{15}N-(2-propenyl)choline, with the enhancement factor of ~3000 and the T_1 time of *ca.* 150 s.[158] Hydrogenation of the triple bond of 5-methyl-5-propargylbarbituric acid yielded hyperpolarized 5-methyl-5-propenylbarbituric acid,[159] which is potentially useful for the studies of pharmaceuticals. Alkyne-functionalized poly(lysine) derivatives with phenylpropiolate or propargylamine moieties were synthesized and tested in PHIP experiments.[160] Hydrogenation of terminal alkyne groups in a biocompatible hyperbranched polymer produced observable polarization in the product despite the potential steric effects and the short relaxation times of the product.[161]

To further extend the range of hyperpolarized substrates, processes more sophisticated than a simple hydrogenation have been suggested. For instance, the hydrogenation of [1-^{13}C]phosphoenolpyruvate, in which the protective phosphate group stabilizes the C=C double bond, to racemic [1-^{13}C]phospholactate was suggested as a potential way to hyperpolarized lactate, assuming that the phosphate moiety can be removed enzymatically after the hydrogenation stage.[162] In another study, maleic anhydride was hydrogenated with parahydrogen to afford hyperpolarized succinic anhydride.[163] The latter was hydrolyzed to hyperpolarized [1-^{13}C]succinate. As both precursor and the catalyst are not soluble in water, the hydrogenation was performed in an organic phase. The signal intensity of succinate after aqueous phase extraction was about 70% of that in the organic phase, and was much larger than that obtained upon aqueous phase hydrogenation of fumaric acid. Substituted alkynes, namely, 2-(2-methoxyethoxy)ethyl phenylpropiolate and bis[2-(2-methoxyethoxy)ethyl]acetylenedicarboxylate, were addressed,[164] with the (oligo)oxyethylenic chains introduced to obtain water-soluble hydrogenation products after the hydrogenation of substrates in an organic phase. After the ^1H to ^{13}C polarization transfer stage, phase transfer by extraction with a small amount of water allowed one to collect ~10% hyperpolarized product in an aqueous phase. The added advantage of extraction-based approaches is that the product is separated from the hydrogenation catalyst. PHIP was also successfully observed in amino acids,[165] and in a peptide upon the hydrogenation of dehydroalanine residues in thiostrepton.[166]

An interesting and important recent development is the observation of PHIP effects in the absence of the incorporation of H atoms into a substrate.[167–170] This effect, termed SABRE, is related to PHIP and originates from the dynamic evolution of the nuclear spin system in a transient intermediate formed by a metal complex catalyst, substrate, and pH_2. As the manifold of coupled nuclear spins involves those of both H atoms and the substrate nuclei, under appropriate conditions this evolution can create an observable hyperpolarization of the bound substrate. A facile exchange of the substrate molecules between the free and the bound states allows a significant number of molecules to be polarized. SABRE significantly broadens the range of molecules that can be polarized using parahydrogen, as contrary to the conventional PHIP, SABRE does not require the synthesis of an unsatutrated precursor that can be hydrogenated with pH_2. Nevertheless, SABRE is still a catalytic process which involves the oxidative addition of H_2 to the catalyst and also crucially depends on the ability of the substrate to coordinate to the metal center of the transition metal complex catalyst, the strength of this binding, *etc*.

7. Extending the lifetime of hyperpolarization beyond the T_1 limit

Despite the enormous progress in sensitivity achieved with the introduction of hyperpolarization techniques, the important disadvantage of hyperpolarized spin states is their transient nature, which limits the time window available for the use and detection of hyperpolarized substances. Hyperpolarization is destroyed by nuclear spin relaxation with a characteristic time T_1, implying that it is reduced by a factor of about 150 every $5\times T_1$ seconds. Until recently, the T_1 was considered to be the ultimate limit for hyperpolarization lifetime. Today, it is clear that this seemingly fundamental limitation can be overcome using the so-called long-lived spin states (LLSS).[171]

An ultimate example of a LLSS is parahydrogen considered above. It is characterized by a singlet spin state of the two hydrogen nuclei with $I = 0$. The interconversion of ortho- ($I = 1$) and parahydrogen can take as long as several months, demonstrating that the characteristic decay time (T_{LLSS}) of LLSS can be much longer than T_1. The spins of several equivalent nuclei can form long-lived spin states in other molecules. However, similar to pH_2, the $I = 0$ state is spinless and thus cannot be directly observed and manipulated in an NMR experiment unless the equivalence of the nuclei is somehow broken. Unfortunately, once this happens, the singlet state is no longer an eigenstate of the spin system and its long-lived character is gone. Therefore, it is essential to switch reversibly between the equivalent (for storage of spin order) and the inequivalent (for manipulations and observations) states of nuclei. This has been achieved using magnetically or chemically nonequivalent nuclei in combination with magnetic field cycling,[172–175] spin-locking with a continuous rf irradiation at high magnetic fields,[176–178] or in a reversible chemical reaction.[179] For molecules with almost equivalent ^{13}C nuclei, the T_{LLSS} times longer than 10 min in solution have been demonstrated.[180] The advantages of combining the properties of the LLSS with hyperpolarization techniques to significantly extend the hyperpolarization lifetime in DNP[181–183] and PHIP[184,185] studies were convincingly demonstrated. The most recent study illustrates an even more surprising fact that hyperpolarization can be used for NMR signal detection, and after that recovered, stored in a singlet state and then used again, with many such cycles possible with a single batch of a hyperpolarized substance.[186]

Conclusions

Dynamic nuclear polarization has become a versatile and widely used technique capable of boosting the sensitivity in various applications of NMR by several orders of magnitude. In particular, significant progress has been achieved in the applications of DNP-enhanced NMR to the studies of enzymatic processes *in vivo* and *in vitro*. Clearly, a combination of hyperpolarization with the use of long-lived spin states can go a long way in significantly extending the time window available for the use of the huge signal enhancement, potentially providing access to a broad range of relatively slow chemical processes. Unfortunately, research in this field in the Russian Federation is essentially nonexistent. This review is intended to attract adequate attention to this area of research and to help change the current situation.

References

1 K. Golman, L. E. Olsson, O. Axelsson, S. Mansson, M. Karlsson and J. S. Petersson, *Brit. J. Radiol*., 2003, **76**, S118.
2 E. Terreno, D. D. Castelli, A. Viale and S. Aime, *Chem. Rev*., 2010, **110**, 3019.
3 P. Bhattacharya, B. D. Ross and R. Bunger, *Exp. Biol. Med*., 2009, **234**, 1395.
4 A. W. Overhauser, *Phys. Rev.*, 1953, **92**, 411.
5 T. R. Carver and C. P. Slichter, *Phys. Rev*., 1953, **92**, 212.
6 A. Abragam and M. Goldman, *Rep. Prog. Phys*., 1978, **41**, 395.
7 K. H. Hausser and D. Stehilk, *Adv. Magn. Reson*., 1968, **3**, 79.
8 T. P. Carver and C. P. Slichter, *Phys. Rev.*, 1956, **102**, 975.
9 M. J. Prandolini, V. P. Denysenkov, M. Gafurov, B. Endeward and T. F. Prisner, *J. Am. Chem. Soc*., 2009, **131**, 6090.
10 M. D. Lingwood, T. A. Siaw, N. Sailasuta, B. D. Ross, P. Bhattacharya and S. Han, *J. Magn. Reson*., 2010, **205**, 247.
11 E. R. McCarney, B. D. Armstrong, M. D. Lingwood and S. Han, *Proc. Natl. Acad. Sci. USA*, 2007, **104**, 1754.
12 J. G. Krummenacker, V. P. Denysenkov and T. F. Prisner, *Appl. Magn. Reson*., 2012, **43**, 139.
13 P. Neugebauer, J. G. Krummenacker, V. P. Denysenkov, G. Parigi, C. Luchinat and T. F. Prisner, *Phys. Chem. Chem. Phys*., 2013, **15**, 6049.
14 U. L. Gunther, *Top. Curr. Chem.*, 2013, **335**, 23.
15 R. G. Griffin and T. F. Prisner, *Phys. Chem. Chem. Phys*., 2010, **12**, 5737.
16 A. V. Atsarkin and W. Kockenberger, *Appl. Magn. Reson.*, 2012, **43**, 1.
17 J. H. Ardenkjaer-Larsen, B. Fridlund, A. Gram, G. Hansson, L. Hansson, M. H. Lerche, R. Servin, M. Thaning and K. Golman, *Proc. Natl. Acad. Sci. USA*, 2003, **100**, 10158.
18 J. Wolber, F. Ellner, B. Fridlund, A. Gram, H. Johannesson, G. Hansson, L. H. Hansson, M. H. Lerche, S. Mansson, R. Servin, M. Thaning, K. Golman and J. H. Ardenkjaer-Larsen, *Nucl. Instr. Meth. Phys. Res. A*, 2004, **526**, 173.
19 J. Leggett, R. Hunter, J. Granwehr, R. Panek, A. J. Perez-Linde, A. J. Horsewill, J. McMaster, G. Smith and W. Kockenberger, *Phys. Chem. Chem. Phys*., 2010, **12**, 5883.
20 S. Hu, P. E. Z. Larson, M. VanCriekinge, A. M. Leach, I. Park, C. Leon, J. Zhou, P. J. Shin, G. Reed, P. Keselman, C. von Morze, H. Yoshihara, R. A. Bok, S. J. Nelson, J. Kurhanewicz and D. B. Vigneron, *Magn. Reson. Imaging*, 2013, **31**, 490.
21 J. H. Ardenkjaer-Larsen, A. M. Leach, N. Clarke, J. Urbahn, D. Anderson and T. W. Skloss, *NMR Biomed.*, 2011, **24**, 927.
22 C. Hilty and S. Bowen, *Org. Biomol. Chem*., 2010, **8**, 3361.
23 F. A. Gallagher, M. I. Kettunen and K. M. Brindle, *Progr. Nucl. Magn. Reson. Spectrosc*., 2009, **55**, 285.
24 Y.-F. Yen, K. Nagasawa and T. Nakada, *Magn. Reson. Med. Sci.*, 2011, **10**, 211.
25 M. Karlsson, P. R. Jensen, J. Ø. Duus, S. Meier and M. H. Lerche, *Appl. Magn. Reson*., 2012, **43**, 223.
26 R. E. Hurd, Y.-F. Yen, A. Chen and J. H. Ardenkjaer-Larsen, *J. Magn. Reson. Imaging*, 2012, **36**, 1314.
27 A. Bornet, R. Melzi, A. J. Perez Linde, P. Hautle, B. van den Brandt, S. Jannin and G. Bodenhausen, *J. Phys. Chem. Lett*., 2013, **4**, 111.
28 T. Harris, C. Bretschneider and L. Frydman, *J. Magn. Reson*., 2011, **211**, 96.
29 S. Bowen and C. Hilty, *Angew. Chem. Int. Ed*., 2008, **47**, 5235.
30 S. Bowen and C. Hilty, *Phys. Chem. Chem. Phys.*, 2010, **12**, 5766.
31 C. von Morze, G. Reed, P. Shin, P. E. Z. Larson, S. Hu, R. Bok and D. B. Vigneron, *J. Magn. Reson*., 2011, **211**, 109.
32 S. Josan, Y.-F. Yen, R. Hurd, A. Pfefferbaum, D. Spielman and D. Mayer, *J. Magn. Reson.*, 2011, **209**, 332.
33 M. Batel, M. Krajewski, A. Dapp, A. Hunkeler, B. H. Meier, S. Kozerke and M. Ernst, *Chem. Phys. Lett*., 2012, **554**, 72.
34 S. Jannin, A. Bornet, R. Melzi and G. Bodenhausen, *Chem. Phys. Lett*., 2012, **549**, 99.
35 D. J. Tyler, *Curr. Cardiovasc. Imaging Rep.*, 2011, **4**, 108.
36 K. Golman and J. S. Petersson, *Acad. Radiol*., 2006, **13**, 932.
37 K. Golman, J. H. Ardenkjaer-Larsen, J. S. Petersson, S. Mansson and I. Leunbach, *Proc. Natl. Acad. Sci. USA*, 2003, **100**, 10435.
38 K. Golman, J. H. Ardenkjaer-Larsen, J. Svensson, O. Axelsson, G. Hansson, L. Hansson, H. Johannesson, I. Leunbach, S. Mansson, J. S. Petersson, G. Pettersson, R. Servin and L. G. Wistrand, *Acad. Radiol*., 2002, **9**, S507.
39 T. H. Witney and K. M. Brindle, *Biochem. Soc. Trans*., 2010, **38**, 1220.
40 A. Viale, F. Reineri, W. Dastru and S. Aime, *Exp. Opinion Med. Diagn.*, 2012, **6**, 335.
41 J. Kurhanewicz, D. B. Vigneron, K. Brindle, E. Y. Chekmenev, A. Comment, C. H. Cunningham, R. J. DeBerardinis, G. G. Green, M. O. Leach, S. S. Rajan, R. R. Rizi, B. D. Ross, W. S. Warren and C. R. Malloy, *Neoplasia*, 2011, **13**, 81.
42 K. M. Brindle, S. E. Bohndiek, F. A. Gallagher and M. I. Kettunen, *Magn. Reson. Med*., 2011, **66**, 505.
43 S. J. Nelson, J. Kurhanewicz, D. B. Vigneron, P. Larson, A. Harzstarck, M. Ferrone, M. van Criekinge, J. Chang, R. Bok, I. Park, G. Reed, L. Carvajal, J. Crane, J. H. Ardenkjaer-Larsen, A. Chen, R. Hurd, L.-I. Odegardstuen and J. Tropp, *Proc. Int. Soc. Magn. Reson. Med*., 2012, **20**, 274.
44 K. Golman, R. in 't Zandt and M. Thaning, *Proc. Natl. Acad. Sci. USA*, 2006, **103**, 11270.
45 J. Tropp, J. M. Lupo, A. Chen, P. Calderon, D. McCune, T. Grafendorfer, E. Ozturk-Isik, P. E. Z. Larson, S. Hu, Y.-F. Yen, F. Robb, R. Bok, R. Schulte, D. Xu, R. Hurd, D. Vigneron and S. Nelson, *J. Magn. Reson*., 2011, **208**, 171.
46 S. J. Kohler, Y. Yen, J. Wolber, A. P. Chen, M. J. Albers, R. Bok, V. Zhang, J. Tropp, S. Nelson, D. B. Vigneron, J. Kurhanewicz and R. E. Hurd, *Magn. Reson. Med*., 2007, **58**, 65.
47 D. J. Tyler, M. A. Schroeder, L. E. Cochlin, K. Clarke and G. K. Radda, *Appl. Magn. Reson*., 2008, **34**, 523.
48 M. Marjanska, I. Iltis, A. A. Shestov, D. K. Deelchand, C. Nelson, K. Ugurbil and P.-G. Henry, *J. Magn. Reson.*, 2010, **206**, 210.
49 D. Mayer, Y.-F. Yen, A. Takahashi, S. Josan, J. Tropp, B. K. Rutt, R. E. Hurd, D. M. Spielman and A. Pfefferbaum, *Magn. Reson. Med*., 2011, **65**, 1228.
50 T. Xu, D. Mayer, M. Gu, Y.-F. Yen, S. Josan, J. Tropp, A. Pfefferbaum, R. Hurd and D. Spielman, *NMR Biomed.*, 2011, **24**, 997.
51 S. Hu, A. P. Chen, M. L. Zierhut, R. Bok, Y.-F. Yen, M. A. Schroeder, R. E. Hurd, S. J. Nelson, J. Kurhanewicz and D. B. Vigneron, *Mol. Imaging Biol*., 2009, **11**, 399.
52 M. I. Kettunen, D. Hu, T. H. Witney, R. McLaughlin, F. A. Gallagher, S. E. Bohndiek, S. E. Day and K. M. Brindle, *Magn. Reson. Med.*, 2010, **63**, 872.
53 D. M. Spielman, D. Mayer, Y.-F. Yen, J. Tropp, R. E. Hurd and A. Pfefferbaum, *Magn. Reson. Med.*, 2009, **62**, 307.
54 M. L. Zierhut, Y.-F. Yen, A. P. Chen, R. Bok, M. J. Albers, V. Zhang, J. Tropp, I. Park, D. B. Vigneron, J. Kurhanewicz, R. E. Hurd and S. J. Nelson, *J. Magn. Reson.*, 2010, **202**, 85.
55 C. Harrison, C. Yang, A. Jindal, R. J. DeBerardinis, M. A. Hooshyar, M. Merritt, A. Dean Sherry and C. R. Malloy, *NMR Biomed.*, 2012, **25**, 1286.
56 T. H. Witney, M. I. Kettunen and K. M. Brindle, *J. Biol. Chem.*, 2011, **286**, 24572.
57 A. P. Chen, R. E. Hurd and C. H. Cunningham, *J. Magn. Reson.*, 2012, **214**, 319.
58 A. P. Chen, M. J. Albers, C. H. Cunningham, S. J. Kohler, Y.-F. Yen, R. E. Hurd, J. Tropp, R. Bok, J. M. Pauly, S. J. Nelson, J. Kurhanewicz and D. B. Vigneron, *Magn. Reson. Med.*, 2007, **58**, 1099.
59 S. J. Nelson, D. Vigneron, J. Kurhanewicz, A. Chen, R. Bok and R. Hurd, *Appl. Magn. Reson.*, 2008, **34**, 533.
60 M. J. Albers, R. Bok, A. P. Chen, C. H. Cunningham, M. L. Zierhut, V. Y. Zhang, S. J. Kohler, J. Tropp, R. E. Hurd, Y. F. Yen, S. J. Nelson, D. B. Vigneron and J. Kurhanewicz, *Cancer Res*., 2008, **68**, 8607.
61 K. Golman, R. in't Zandt, M. Lerche, R. Pehrson and J. H. Ardenkjaer-Larsen, *Cancer Res*., 2006, **66**, 10855.
62 M. M. Darpolor, Y.-F. Yen, M.-S. Chua, L. Xing, R. H. Clarke-Katzenberg, W. Shi, D. Mayer, S. Josan, R. E. Hurd, A. Pfefferbaum, L. Senadheera, S. So, L. V. Hofmann, G. M. Glazer and D. M. Spielman, *NMR Biomed.*, 2011, **24**, 506.

63 Y.-F. Yen, P. Le Roux, D. Mayer, R. King, D. Spielman, J. Tropp, K. B. Pauly, A. Pfefferbaum, S. Vasanawala and R. Hurd, *NMR Biomed*., 2010, **23**, 414.
64 H. Dafni, P. E. Z. Larson, S. Hu, H. A. I. Yoshihara, C. S. Ward, H. S. Venkatesh, C. Wang, X. Zhang, D. B. Vigneron and S. M. Ronen, *Cancer Res.*, 2010, **70**, 7400.
65 P. Seth, A. Grant, J. Tang, E. Vinogradov, X. Wang, R. Lenkinski and V. P. Sukhatme, *Neoplasia*, 2011, **13**, 60.
66 I. Park, P. E. Z. Larson, M. L. Zierhut, S. Hu, R. Bok, T. Ozawa, J. Kurhanewicz, D. B. Vigneron, S. R. VandenBerg, C. D. James and S. J. Nelson, *Neuro-Oncology*, 2010, **12**, 133.
67 C. S. Ward, H. S. Venkatesh, M. M. Chaumeil, A. H. Brandes, M. Van Criekinge, H. Dafni, S. Sukumar, S. J. Nelson, D. B. Vigneron, J. Kurhanewicz, C. D. James, D. A. Haas-Kogan and S. M. Ronen, *Cancer Res.*, 2010, **70**, 1296.
68 S. E. Day, M. I. Kettunen, F. A. Gallagher, D.-E. Hu, M. Lerche, J. Wolber, K. Golman, J. H. Ardenkjaer-Larsen and K. M. Brindle, *Nature Med*., 2007, **13**, 1382.
69 S. Hu, A. Balakrishnan, R. B. A. Bok, B. Anderton, P. B. E. Z. Larson, S. B. J. Nelson, J. Kurhanewicz, D. B. B. Vigneron and A. Goga, *Cell Metab*., 2011, **14**, 131.
70 T. R. Eykyn, R. Southworth and S. Kozerke, *Heart Metab.*, 2012, **55**, 13.
71 M. A. Schroeder, K. Clarke, S. Neubauer and D. J. Tyler, *Circulation*, 2011, **124**, 1580.
72 K. Golman, J. S. Petersson, P. Magnusson, E. Johansson, P. Akeson, C. M. Chai, G. Hansson and S. Mansson, *Magn. Reson. Med*., 2008, **59**, 1005.
73 M. A. Schroeder, L. E. Cochlin, L. C. Heather, K. Clarke, G. K. Radda and D. J. Tyler, *Proc. Natl. Acad. Sci. USA*, 2008, **105**, 12051.
74 H. J. Atherton, M. A. Schroeder, M. S. Dodd, L. C. Heather, E. E. Carter, L. E. Cochlin, S. Nagel, N. R. Sibson, G. K. Radda, K. Clarke and D. J. Tyler, *NMR Biomed.*, 2011, **24**, 201.
75 L. Menichetti, F. Frijia, A. Flori, F. Wiesinger, V. Lionetti, G. Giovannetti, G. D. Aquaro, F. A. Recchia, J. H. Ardenkjaer-Larsen, M. F. Santarelli and M. Lombardi, *Contrast Media Mol. Imaging*, 2012, **7**, 85.
76 M. A. Schroeder, H. J. Atherton, D. R. Ball, M. A. Cole, L. C. Heather, J. L. Griffin, K. Clarke, G. K. Radda and D. J. Tyler, *FASEB J*., 2009, **23**, 2529.
77 M. S. Dodd, D. R. Ball, M. A. Schroeder, L. M. Le Page, H. J. Atherton, L. C. Heather, A.-M. Seymour, H. Ashrafian, H. Watkins, K. Clarke and D. J. Tyler, *Cardiovasc. Res*., 2012, **95**, 69.
78 A. P. Chen, R. E. Hurd, M. A. Schroeder, A. Z. Lau, Y. Gu, W. W. Lam, J. Barry, J. Tropp and C. H. Cunningham, *NMR Biomed.*, 2012, **25**, 305.
79 M. A. Schroeder, P. Swietach, H. J. Atherton, F. A. Gallagher, P. Lee, G. K. Radda, K. Clarke and D. J. Tyler, *Cardiovasc. Res.*, 2009, **86**, 82.
80 M. E. Merritt, C. Harrison, A. D. Sherry, C. R. Malloy and S. C. Burgess, *Proc. Natl. Acad. Sci. USA*, 2011, **108**, 19084.
81 R. E. Hurd, Y.-F. Yen, D. Mayer, A. Chen, D. Wilson, S. Kohler, R. Bok, D. Vigneron, J. Kurhanewicz, J. Tropp, D. Spielman and A. Pfefferbaum, *Magn. Reson. Med*., 2010, **63**, 1137.
82 P. R. Jensen, M. Karlsson, S. Meier, J. Duus and M. H. Lerche, *Chem. Eur. J*., 2009, **15**, 10010.
83 S. Hu, M. Zhu, H. A. I. Yoshihara, D. M. Wilson, K. R. Keshari, P. Shin, G. Reed, C. von Morze, R. Bok, P. E. Z. Larson, J. Kurhanewicz and D. B. Vigneron, *Magn. Reson. Imaging*, 2011, **29**, 1035.
84 F. A. Gallagher, M. I. Kettunen, S. E. Day, D.-E. Hu, M. Karlsson, A. Gisselsson, M. H. Lerche and K. M. Brindle, *Magn. Reson. Med*., 2011, **66**, 18.
85 A. P. Chen, J. Kurhanewicz, R. Bok, D. Xu, D. Joun, V. Zhang, S. J. Nelson, R. E. Hurd and D. B. Vigneron, *Magn. Reson. Imaging*, 2008, **26**, 721.
86 D. Mayer, Y.-F. Yen, S. Josan, J. M. Park, A. Pfefferbaum, R. E. Hurd and D. M. Spielman, *NMR Biomed.*, 2012, **25**, 1119.
87 F. A. Gallagher, M. I. Kettunen, S. E. Day, D.-E. Hu, J. H. Ardenkjær-Larsen, R. in't Zandt, P. R. Jensen, M. Karlsson, K. Golman, M. H. Lerche and K. M. Brindle, *Nature*, 2008, **453**, 940.
88 F. A. Gallagher, M. I. Kettunen and K. M. Brindle, *NMR Biomed.*, 2011, **24**, 1006.
89 D. M. Wilson, K. R. Keshari, P. E. Z. Larson, A. P. Chen, S. Hu, M. Van Criekinge, R. Bok, S. J. Nelson, J. M. Macdonald, D. B. Vigneron and J. Kurhanewicz, *J. Magn. Reson*., 2010, **205**, 141.
90 F. A. Gallagher, M. I. Kettunen, D.-E. Hu, P. R. Jensen, R. in't Zandt, M. Karlsson, A. Gisselsson, S. K. Nelson, T. H. Witney, S. E. Bohndiek, G. Hansson, T. Peitersen, M. H. Lerche and K. M. Brindle, *Proc. Natl. Acad. Sci. USA*, 2009, **106**, 19801.
91 S. E. Bohndiek, M. I. Kettunen, D.-E. Hu, T. H. Witney, B. W. C. Kennedy, F. A. Gallagher and K. M. Brindle, *Mol. Cancer. Ther*., 2010, **9**, 3278.
92 T. H. Witney, M. I. Kettunen, D.-E. Hu, F. A. Gallagher, S. E. Bohndiek, R. Napolitano and K. M. Brindle, *Brit. J. Cancer*, 2010, **103**, 1400.
93 K. R. Keshari, D. M. Wilson, A. P. Chen, R. Bok, P. E. Z. Larson, S. Hu, M. Van Criekinge, J. M. Macdonald, D. B. Vigneron and J. Kurhanewicz, *J. Am. Chem. Soc*., 2009, **131**, 17591.
94 M. Mishkovsky, A. Comment and R. Gruetter, *J. Cerebral Blood Flow Metab*., 2012, **32**, 2108.
95 M. Mishkovsky, T. Cheng, A. Comment and R. Gruetter, *Magn. Reson. Med*., 2012, **68**, 349.
96 S. E. Bohndiek, M. I. Kettunen, D.-E. Hu, B. W. C. Kennedy, J. Boren, F. A. Gallagher and K. M. Brindle, *J. Am. Chem. Soc*., 2011, **133**, 11795.
97 K. R. Keshari, J. Kurhanewicz, R. Bok, P. E. Z. Larson, D. B. Vigneron and D. M. Wilson, *Proc. Natl. Acad. Sci. USA*, 2011, **108**, 18606.
98 K. R. Keshari, J. Kurhanewicz, R. E. Jeffries, D. M. Wilson, B. J. Dewar, M. Van Criekinge, M. Zierhut, D. B. Vigneron and J. M. Macdonald, *Magn. Reson. Med.*, 2010, **63**, 322.
99 T. Harris, G. Eliyahu, L. Frydman and H. Degani, *Proc. Natl. Acad. Sci. USA*, 2009, **106**, 18131.
100 A. W. Barb, S. K. Hekmatyar, J. N. Glushka and J. H. Prestegard, *J. Magn. Reson*., 2013, **228**, 59.
101 P. R. Jensen, S. Meier, J. H. Ardenkjær-Larsen, J. Ø. Duus, M. Karlsson and M. H. Lerche, *Chem. Commun.*, 2009, 5168.
102 F. A. Gallagher, M. I. Kettunen, S. E. Day, M. Lerche and K. M. Brindle, *Magn. Reson. Med*., 2008, **60**, 253.
103 C. Gabellieri, S. Reynolds, A. Lavie, G. S. Payne, M. O. Leach and T. R. Eykyn, *J. Am. Chem. Soc*., 2008, **130**, 4598.
104 R. Sarkar, A. Comment, P. R. Vasos, S. Jannin, R. Gruetter, G. Bodenhausen, H. Hall, D. Kirik and V. P. Denisov, *J. Am. Chem. Soc*., 2009, **131**, 16014.
105 T. Harris, P. Giraudeau and L. Frydman, *Chem. Eur. J*., 2011, **17**, 697.
106 Y. Jamin, C. Gabellieri, L. Smyth, S. Reynolds, S. P. Robinson, C. J. Springer, M. O. Leach, G. S. Payne and T. R. Eykyn, *Magn. Reson. Med*., 2009, **62**, 1300.
107 S. Meier, M. Karlsson, P. R. Jensen, M. H. Lerche and J. O. Duus, *Mol. Biosyst*., 2011, **7**, 2834.
108 S. Meier, P. R. Jensen and J. Ø. Duus, *FEBS Lett.*, 2011, **585**, 3133.
109 S. Meier, P. R. Jensen and J. Ø. Duus, *ChemBioChem*, 2012, **13**, 308.
110 A. P. Chen, R. E. Hurd, Y. Gu, D. M. Wilson and C. H. Cunningham, *NMR Biomed*., 2011, **24**, 514.
111 H. Zeng, Y. Lee and C. Hilty, *Anal. Chem*., 2010, **82**, 8897.
112 Y. Lee, G. S. Heo, H. Zeng, K. L. Wooley and C. Hilty, *J. Am. Chem. Soc*., 2013, **135**, 4636.
113 A. R. Lippert, K. R. Keshari, J. Kurhanewicz and C. J. Chang, *J. Am. Chem. Soc*., 2011, **133**, 3776.
114 T. Doura, R. Hata, H. Nonaka, K. Ichikawa and S. Sando, *Angew. Chem. Int. Ed*., 2012, **51**, 10114.
115 G. Zhang, F. Schilling, S. J. Glaser and C. Hilty, *Anal. Chem*., 2013, **85**, 2875.
116 M. Mishkovsky and L. Frydman, *ChemPhysChem*, 2008, **9**, 2340.
117 C.-G. Joo, A. Casey, C. J. Turner and R. G. Griffin, *J. Am. Chem. Soc*., 2009, **131**, 12.
118 D. M. Wilson, R. E. Hurd, K. Keshari, M. Van Criekinge, A. P. Chen, S. J. Nelson, D. B. Vigneron and J. Kurhanewicz, *Proc. Natl. Acad. Sci. USA*, 2009, **106**, 5503.
119 M. H. Lerche, S. Meier, P. R. Jensen, S. O. Hustvedt, M. Karlsson, J. Ø. Duus and J. H. Ardenkjaer-Larsen, *NMR Biomed*., 2011, **24**, 96.
120 M. Ragavan, H.-Y. Chen, G. Sekar and C. Hilty, *Anal. Chem.*, 2011, **83**, 6054.
121 M. Lelli, D. Gajan, A. Lesage, M. A. Caporini, V. Vitzthum, P. Mieville, F. Heroguel, F. Rascon, A. Roussey, C. Thieuleux, M. Boualleg, L. Veyre, G. Bodenhausen, C. Coperet and L. Emsley, *J. Am. Chem. Soc.*, 2011, **133**, 2104.
122 M. H. Lerche, S. Meier, P. R. Jensen, H. Baumann, B. O. Petersen, M. Karlsson, J. O. Duus and J. H. Ardenkjaer-Larsen, *J. Magn. Reson*., 2010, **203**, 52.
123 A. B. Barnes, G. De Paepe, P. C. A. van der Wel, K.-N. Hu, C.-G. Joo, V. S. Bajaj, M. L. Mak-Jurkauskas, J. R. Sirigiri, J. Herzfeld, R. J. Temkin and R. G. Griffin, *Appl. Magn. Reson*., 2008, **34**, 237.
124 M. Rosay, L. Tometich, Sh. Pawsey, R. Bader, R. Schauwecker, M. Blank, Ph. M. Borchard, S. R. Cauffman, K. L. Felch, R. T. Weber, R. J. Temkin, R. G. Griffin and W. E. Maas, *Phys. Chem. Chem. Phys*., 2010, **12**, 5850.
125 R. A. Green, R. W. Adams, S. B. Duckett, R. E. Mewis, D. C. Williamson and G. G. R. Green, *Prog. Nucl. Magn. Reson. Spectrosc*., 2012, **67**, 1.
126 C. R. Bowers and D. P. Weitekamp, *J. Am. Chem. Soc*., 1987, **109**, 5541.
127 J. Natterer and J. Bargon, *Prog. Nucl. Magn. Reson. Spectrosc*., 1997, **31**, 293.
128 D. Canet, C. Aroulanda, P. Mutzenhardt, S. Aime, R. Gobetto and F. Reineri, *Concepts Magn. Reson.*, 2006, **28A**, 321.
129 S. B. Duckett and N. J. Wood, *Coord. Chem. Rev.*, 2008, **252**, 2278.
130 H. G. Niessen, D. Schleyer, S. Wiemann, J. Bargon, S. Steiner and B. Driessen-Holscher, *Magn. Reson. Chem.*, 2000, **38**, 747.

131 S. B. Duckett and R. E. Mewis, *Acc. Chem. Res*., 2012, **45**, 1247.
132 K. V. Kovtunov, V. V. Zhivonitko, I. V. Skovpin, D. A. Barskiy and I. V. Koptyug, *Top. Curr. Chem*., 2013, **338**, 123.
133 I. V. Koptyug, K. V. Kovtunov, S. R. Burt, M. S. Anwar, C. Hilty, S. Han, A. Pines and R. Z. Sagdeev, *J. Am. Chem. Soc*., 2007, **129**, 5580.
134 K. V. Kovtunov, V. V. Zhivonitko, A. Corma and I. V. Koptyug, *J. Phys. Chem. Lett*., 2010, **1**, 1705.
135 I. V. Skovpin, V. V. Zhivonitko and I. V. Koptyug, *Appl. Magn. Reson*., 2011, **41**, 393.
136 I. V. Skovpin, V. V. Zhivonitko, R. Kaptein and I. V. Koptyug, *Appl. Magn. Reson*., 2012, **44**, 289.
137 K. V. Kovtunov, I. E. Beck, V. I. Bukhtiyarov and I. V. Koptyug, *Angew. Chem. Int. Ed*., 2008, **47**, 1492.
138 K. V. Kovtunov, V. V. Zhivonitko, L. Kiwi-Minsker and I. V. Koptyug, *Chem. Commun.*, 2010, **46**, 5764.
139 D. A. Barskiy, K. V. Kovtunov, A. Primo, A. Corma, R. Kaptein and I. V. Koptyug, *ChemCatChem*, 2012, **4**, 2031.
140 V. V. Zhivonitko, K. V. Kovtunov, I. E. Beck, A. B. Ayupov, V. I. Bukhtiyarov and I. V. Koptyug, *J. Phys. Chem. C*, 2011, **115**, 13386.
141 K. V. Kovtunov, I. E. Beck, V. V. Zhivonitko, D. A. Barskiy, V. I. Bukhtiyarov and I. V. Koptyug, *Phys. Chem. Chem. Phys.*, 2012, **14**, 11008.
142 L.-S. Bouchard, S. R. Burt, M. S. Anwar, K. V. Kovtunov, I. V. Koptyug and A. Pines, *Science*, 2008, **319**, 442.
143 V. V. Zhivonitko, V.-V. Telkki and I. V. Koptyug, *Angew. Chem. Int. Ed*., 2012, **51**, 8054.
144 K. Golman, O. Axelsson, H. Johannesson, S. Mansson, C. Olofsson and J. S. Petersson, *Magn. Reson. Med.*, 2001, **46**, 1.
145 E. Y. Chekmenev, J. Hovener, V. A. Norton, K. Harris, L. S. Batchelder, P. Bhattacharya, B. D. Ross and D. P. Weitekamp, *J. Am. Chem. Soc*., 2008, **130**, 4212.
146 E. Y. Chekmenev, V. A. Norton, D. P. Weitekamp and P. Bhattacharya, *J. Am. Chem. Soc*., 2009, **131**, 3164.
147 J.-B. Hovener, E. Y. Chekmenev, K. C. Harris, W. H. Perman, T. T. Tran, B. D. Ross and P. Bhattacharya, *MAGMA*, 2009, **22**, 123.
148 P. Bhattacharya, E. Y. Chekmenev, W. H. Perman, K. C. Harris, A. P. Lin, V. A. Norton, C. T. Tan, B. D. Ross and D. P. Weitekamp, *J. Magn. Reson.*, 2007, **186**, 150.
149 B. D. Ross, P. Bhattacharya, S. Wagner, T. Tran and N. Sailasuta, *Am. J. Neuroradiol*., 2010, **31**, 24.
150 N. M. Zacharias, H. R. Chan, N. Sailasuta, B. D. Ross and P. Bhattacharya, *J. Am. Chem. Soc*., 2012, **134**, 934.
151 H. Johannesson, O. Axelsson and M. Karlsson, *C.R. Phys.*, 2004, **5**, 315.
152 M. Goldman, H. Johannesson, O. Axelsson and M. Karlsson, *Magn. Reson. Imaging*, 2005, **23**, 153.
153 M. Goldman, H. Johannesson, O. Axelsson and M. Karlsson, *C.R. Chim.*, 2006, **9**, 357.
154 M. Goldman and H. Johannesson, *C.R. Phys*., 2005, **6**, 575.
155 J.-B. Hovener, E. Y. Chekmenev, K. C. Harris, W. H. Perman, L. W. Robertson, B. D. Ross and P. Bhattacharya, *MAGMA*, 2009, **22**, 111.
156 A. Gamliel, H. Allouche-Arnon, R. Nalbandian, C. M. Barzilay, J. M. Gomori and R. Katz-Brull, *Appl. Magn. Reson*., 2010, **39**, 329.
157 F. Reineri, D. Santelia, A. Viale, E. Cerutti, L. Poggi, T. Tichy, S. S. D. Premkumar, R. Gobetto and S. Aime, *J. Am. Chem. Soc*., 2010, **132**, 7186.
158 F. Reineri, A. Viale, S. Ellena, D. Alberti, T. Boi, G. B. Giovenzana, R. Gobetto, S. S. D. Premkumar and S. Aime, *J. Am. Chem. Soc.*, 2012, **134**, 11146.
159 M. Roth, A. Koch, P. Kindervater, J. Bargon, H. W. Spiess and K. Munnemann, *J. Magn. Reson*., 2010, **204**, 50.
160 S. Aime, W. Dastru, R. Gobetto and A. Viale, *Org. Biomol. Chem*., 2005, **3**, 3948.
161 K. Munnemann, M. Kolzer, I. Blakey, A. K. Whittaker and K. J. Thurecht, *Chem. Commun*., 2012, **48**, 1583.
162 R. V. Shchepin, A. M. Coffey, K. W. Waddell and E. Y. Chekmenev, *J. Am. Chem. Soc*., 2012, **134**, 3957.
163 F. Reineri, A. Viale, S. Ellena, T. Boi, V. Daniele, R. Gobetto and S. Aime, *Angew. Chem. Int. Ed*., 2011, **50**, 7350.
164 F. Reineri, A. Viale, G. Giovenzana, D. Santelia, W. Dastru, R. Gobetto and S. Aime, *J. Am. Chem. Soc*., 2008, **130**, 15047.
165 S. Wildschutz, P. Hubler and J. Bargon, *ChemPhysChem*, 2001, **2**, 328.
166 F. Gruppi, X. Xu, B. Zhang, J. A. Tang, A. Jerschow and J. W. Canary, *Angew. Chem. Int. Ed.*, 2012, **51**, 11787.
167 R. W. Adams, J. A. Aguilar, K. D. Atkinson, M. J. Cowley, P. I. P. Elliott, S. B. Duckett, G. G. R. Green, I. G. Khazal, J. Lopez-Serrano and D. C. Williamson, *Science*, 2009, **323**, 1708.
168 K. D. Atkinson, M. J. Cowley, P. I. P. Elliott, S. B. Duckett, G. G. R. Green, J. Lopez-Serrano and A. C. Whitwood, *J. Am. Chem. Soc*., 2009, **131**, 13362.
169 K. D. Atkinson, M. J. Cowley, S. B. Duckett, P. I. P. Elliott, G. G. R. Green, J. Lopez-Serrano, I. G. Khazal and A. C. Whitwood, *Inorg. Chem*., 2009, **48**, 663.
170 M. J. Cowley, R. W. Adams, K. D. Atkinson, M. C. R. Cockett, S. B. Duckett, G. G. R. Green, J. A. B. Lohman, R. Kerssebaum, D. Kilgour and R. E. Mewis, *J. Am. Chem. Soc.*, 2011, **133**, 6134.
171 M. H. Levitt, *Annu. Rev. Phys. Chem.*, 2012, **63**, 89.
172 M. Carravetta, O. G. Johannessen and M. H. Levitt, *Phys. Rev. Lett*., 2004, **92**, 153003-1.
173 M. Carravetta and M. H. Levitt, *J. Chem. Phys*., 2005, **122**, 214505.
174 G. Pileio, M. Carravetta and M. H. Levitt, *Proc. Natl. Acad. Sci. USA*, 2010, **107**, 17135.
175 G. Pileio, M. Carravetta, E. Hughes and M. H. Levitt, *J. Am. Chem. Soc*., 2008, **130**, 12582.
176 K. Gopalakrishnan and G. Bodenhausen, *J. Magn. Reson.*, 2006, **182**, 254.
177 M. Carravetta and M. H. Levitt, *J. Am. Chem. Soc.*, 2004, **126**, 6228.
178 G. Pileio and M. H. Levitt, *J. Chem. Phys.*, 2009, **130**, 214501.
179 W. S. Warren, E. Jenista, R. T. Branca and X. Chen, *Science*, 2009, **323**, 1711.
180 G. Pileio, J. T. Hill-Cousins, S. Mitchell, I. Kuprov, L. J. Brown, R. C. D. Brown and M. H. Levitt, *J. Am. Chem. Soc*., 2012, **134**, 17494.
181 P. Ahuja, R. Sarkar, S. Jannin, P. R. Vasos and G. Bodenhausen, *Chem. Commun.*, 2010, **46**, 8192.
182 P. R. Vasos, A. Comment, R. Sarkar, P. Ahuja, S. Jannin, J.-P. Ansermet, J. A. Konter, P. Hautle, B. Van Den Brandt and G Bodenhausen, *Proc. Natl. Acad. Sci. USA*, 2009, **106**, 18469.
183 C. Laustsen, G. Pileio, M. C. D. Tayler, L. J. Brown, R. C. D. Brown, M. H. Levitt and J. H. Ardenkjaer-Larsen, *Magn. Reson. Med.*, 2012, **68**, 1262.
184 M. B. Franzoni, L. Buljubasich, H. W. Spiess and K. Munnemann, *J. Am. Chem. Soc.*, 2012, **134**, 10393.
185 E. Vinogradov and A. K. Grant, *J. Magn. Reson*., 2008, **194**, 46.
186 G. Pileio, S. Bowen, C. Laustsen, M. C. D. Tayler, J. T. Hill-Cousins, L. J. Brown, R. C. D. Brown, J. H. Ardenkjaer-Larsen and M. H. Levitt, *J. Am. Chem. Soc*., 2013, **135**, 5084.

Received: 25th June 2013; Com. 13/4141